Doctoral Dissertation

Development of Envelope-Type Lipid-Coated Gold Nanorods for Anti-Cancer Photothermal Therapy

(癌の光熱療法を目指した脂質エンベロープ型金ナノロッドの創製)

Laboratory for Molecular Design of Pharmaceutics

Faculty of Pharmaceutical Sciences

Graduate School of Life Science

Hokkaido University

West Kristian D. Paraiso

Sapporo, Japan

September 2017

Acknowledgement

"Alle Reisen haben eine heimliche Bestimmung, die der Reisende nicht annt."

(All journeys have a secret destination of which the traveler is unaware.)

-Martin Buber (1878-1965), Austrian Philosopher

More than three years ago, I came to Japan with the intention of simply learning all I can about drug delivery systems research. However, I did not expect that I would be learning so much more aside from theories and laboratory techniques. I am now convinced that a doctorate is only 50% about your dissertation and 50% about discovering yourself and fixing your shortcomings. One of the most important things that I have learned in this journey is how you can be stronger by learning to accept all of your weaknesses and trying to correct them even if it is not an easy thing to do. And this is a lesson that I will carry with me long after I leave Japan.

This doctoral work would not have been possible without the guidance of my adviser, **Professor Hideyoshi Harashima**, who believed in me and took me under his wing despite initially not having a background in drug delivery systems. I am grateful for all the discussions with him through the years, where he always showed his broad perspective on research on drug delivery and nanomedicine. His support for my endeavors in attending conferences and pursuing career interests are also well appreciated.

My heartfelt gratitude also goes out to my direct supervisor, **Professor Hidetaka Akita** (Chiba University), for introducing me to research on gold nanorods and liposome-based delivery systems, accompanying me on learning how to use several instruments, introducing me to people who can help with the experiments, guiding me in many graduate school procedures, correcting my manuscripts, and constantly pushing me to do my best in my research.

I am also thankful for my second supervisor, **Dr. Yusuke Sato**, for teaching me experiments in organic synthesis and *in vivo* pharmacokinetics; my former senior lab colleague, **Dr. Hiroki Tanaka** (Chiba University), for teaching me many of the techniques I used in my research, including liposome preparation, cell culture, animal handling, and for performing ICP-AES measurements of gold concentrations; my former colleagues in the Akita group: **Ayaka Watanabe**, **Mio Maeta**, and **Naoya Miura**, for guiding me through many exploratory experiments with ssPalm; all the former and present staff in our laboratory, **Dr. Yuma Yamada**, **Dr. Kazuaki Kajimoto**, **Dr. Takashi Nakamura**, **Dr. Yu Sakurai**, and **Dr.**

Ikramy Khalil, for the constructive comments on my seminars and other presentations through the years; and the lab secretaries, **Ms. Eiko Abe** and **Ms. Eriko Kano**, for helping me navigate the many complicated procedures in graduate school.

My gratitude goes to **Professor Katsumi Maenaka** as well for agreeing to chair my dissertation panel and for evaluating this doctoral work.

I truly appreciate the friendship and intellectual discussions with my other foreign lab colleagues, which kept me sane during our time together. I would like to thank **Sa'ed Abassi**, for teaching me FACS and all the quick insightful chats about research and about life, in general; **Nour Shobaki**, for patiently sharing her knowledge and experience on mice handling and *in vivo* experiments; my batchmate, **Sarochin Santiwarangkool**, for being always open for questions not only about experiments, but also those with regards to Japanese documents; **Laila Burger**, for the occasional help with cell culture and for encouraging me to learn German; and **Dr. Lewis Lee**, for always offering advice regarding the chemistry of nanoparticles.

I would also like to thank **Dr. Kenichi Niikura** (Research Institute for Electronic Science), for sharing his protocol on gold uptake analysis and **Ms. Naomi Kawai** (Hokkaido University Open Facility) for initially assisting me with TEM measurements.

I likewise would like to recognize **Dr. Harue Ishii** (Institute for International Collaboration) for helping me deal with the psychological difficulties I encountered while doing my graduate research.

Finally, I am extremely thankful for the support, inspiration, and encouragement from my family, former colleagues and mentors, and friends who I have met along the way, here in Japan and in other countries. I especially thank **Dr. Jose Quinsaat**, and **Dr. Roger Tan** for all the discussions and exchange of ideas in nanoparticle coatings, **Jeffrey Estipular** for helping me with the statistical analyses in my experiments, and my closest friends: **Christine Pineda**, **Dr. Karen Tan**, **Fred Santiañez**, **Kaye Vergel**, **Rachael Lopez**, **Dr. Julius Lopez**, **Dr. Loida Casalme**, **Fatima Cruz**, **Benjamin Magallon**, and **Delburg Mitchao** (Titas), not only for sharing with me wonderful memories but also for helping me get through some very difficult and frustrating times. Your love and friendship will be among the best things I will take with me from Sapporo.

To everyone who gets repeatedly smashed into pieces but still finds the courage each time to get up, put those pieces back together, and try again

Abstract

Photothermal therapy (PTT) is currently an auspicious approach in treating cancer. This is exemplified by the use of gold nanorods (AuNRs) that produce heat in response to near infrared (NIR) irradiation. AuNRs are commonly prepared by using a highly toxic surfactant, cetyltrimethylammonium bromide (CTAB). Because of this, it is necessary to remove traces of CTAB while stabilizing the AuNR surface. In this study, the encapsulation of AuNR in liposome to improve biocompatibility, is reported. To develop this AuNR-multifunctional envelope-type nano device (AuNR-MEND), an SS-cleavable and pH-activated lipid-like material was employed as a component of the lipid envelope. Several methods were attempted in the process of encapsulation. Here, AuNRs were stabilized with bovine serum albumin (AuNR-BSA), and then further encapsulated in the lipid envelope through ethanol dilution method. Change in the ζ-potential of the nanoparticles verified the modifications in coating. Encapsulation was confirmed by transmission electron microscopy (TEM) images. More importantly, the intrinsic properties of AuNRs in terms of heat production in response to NIR irradiation was retained after AuNR-MEND preparation.

The *in vitro* photothermal cytotoxicity of the AuNR-MEND was further demonstrated in 4T1 mouse breast cancer cells. After NIR radiation (750–900 nm) at 1 W/cm^2 for six minutes, the temperature of the medium was increased to approximately 60°C, and cell viability was drastically decreased to approximately 11%. However, this cytotoxic effect cannot be explained simply using temperature increase, since incubation of cells in medium that had been pre-warmed at 60°C resulted in a slight decrease in viability (to approximately 70%). Intracellular delivery of the AuNRs therefore is a key factor for the high photothermal cytotoxicity. At a low dose, the photothermal cytotoxicity of AuNR-BSA was higher than that of AuNR-MEND. In contrast, a higher dose of AuNR-MEND resulted in the complete destruction of the cells when subjected to NIR irradiation, while the cell survival rate reached a plateau at 30% in the case of AuNR-BSA. Cellular uptake of AuNR-MEND was shown to be dose-dependent and efficient. Moreover, the increase in caspase-3 production suggests that apoptosis was induced after treatment with the nanoparticles.

As for the *in vivo* study, AuNR-MEND was shown to be long circulating, tumor-accumulating, and non-hepatotoxic in BALB/c mice. Thus, delivering AuNR by means of functionalized lipid nanoparticles represents a promising approach to induce NIR-triggered apoptosis without non-specific cytotoxicity. This doctoral work offers an innovative concept of AuNR-encapsulation into the lipid particle for applications of future tumor photothermal therapy.

Summary of Figures and Schemes

Scheme number	**Description**

Table of Contents

Chapter I: General Introduction and Research Objectives

A. Bulk and colloidal gold have different properties

Gold is known as the king of all elements. Because of its lack of reactivity, many historical artifacts, coinage, and jewelry are made from it (**Figure 1-1-a**). It also conducts electricity well, hence its wide use in electronics[1]. On the other hand, colloidal gold has different properties, interacting with visible light to produce brilliant colors. Because of this, early artists used them for stained glass windows (**Figure 1-1-b**). Today, this property of gold nanoparticles have been harnessed by scientists by controlling size, shape, and surface chemistry[2] (**Figure 1-1-c**), making them invaluable to nanomedicine. Nanomedicine is the application of nanotechnology to the biomedical sciences[3]. One gold nanoparticle used as a delivery system for TNF-α is already in clinical development[4]. As of the moment, gold nanoparticles have been synthesized in a variety of shapes: spheres, cages, cubes, frames, rods, and many others[1]. Gold nanorods, because of its unique absorbance property, is the focus of this study.

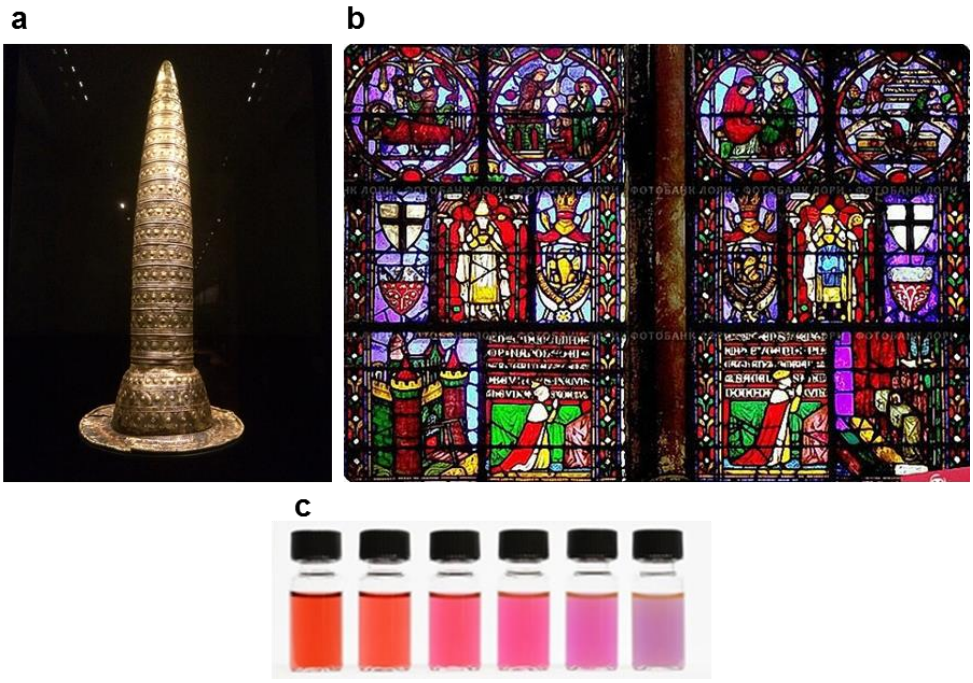

Figure 1-1. Different forms of gold in art and reagents. (a) The Golden Hat, Neues Museum, Berlin (photo taken by the author). (b) A vitrage (stained glass window, photo from EPFL website)[5]. (c) Solutions of gold nanoparticles of various sizes (photo from Sigma-Aldrich website)[2].

B. Gold nanorods are used in photothermal therapy (PTT)

The properties of gold nanorods (AuNRs) are distinct compared to other gold nanoparticles. They absorb near-infrared (NIR) light at around 800 nm because of the longitudinal oscillation of electrons[6], a phenomenon known as surface plasmon resonance (SPR)[7], and rapidly and efficiently convert it to heat through non-radioactive processes, involving electron-electron and electron-photon coupling[8]. This property of AuNRs are used for a non-invasive therapeutic strategy called photothermal therapy (PTT)[9].

PTT using AuNRs has been used for cancer therapy[1] because heat directly damages cancer cells and also improves the efficacy and delivery of chemotherapeutic drugs[10,11] (**Figure 1-2**). The absorption of AuNRs in the NIR region is especially helpful because 650 to 900 nm wavelength light—called the NIR biological window—can penetrate tissues owing to the minimal absorption of water and blood components like hemoglobin (**Figure 1-3**) [12,13].

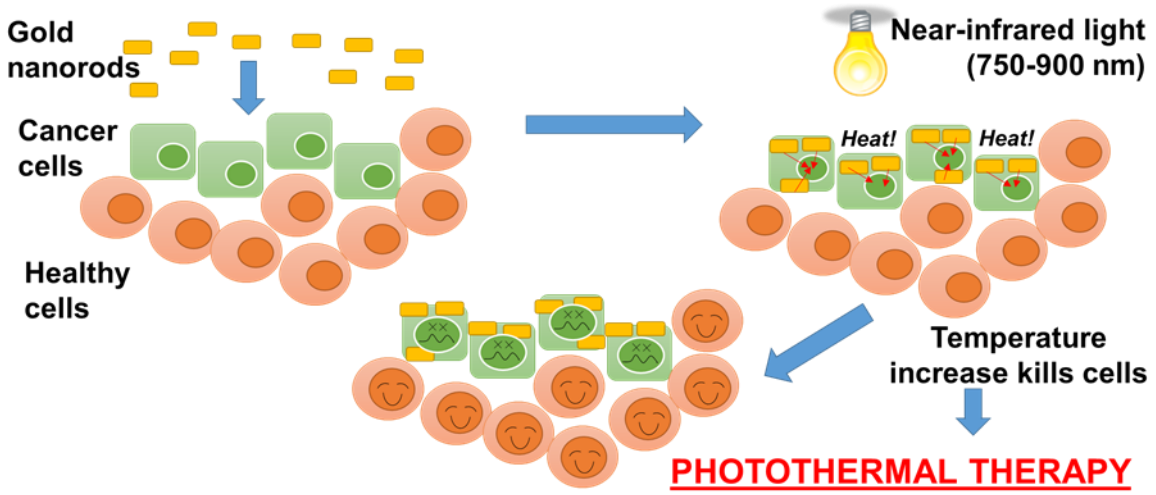

Figure 1-2. Illustration of anti-cancer photothermal therapy (PTT). AuNRs enter cancer cells, absorb NIR light and convert it to heat, killing the cells.

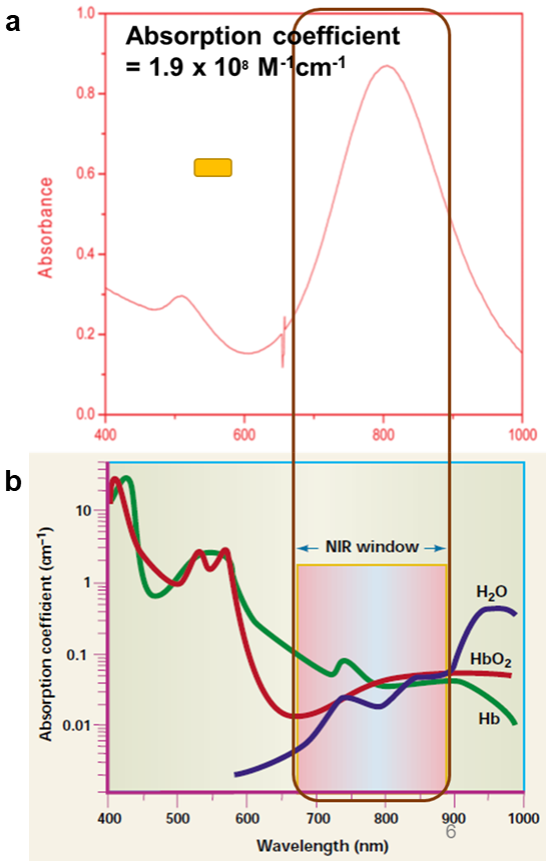

Figure 1-3. Relationship of absorption profile of gold nanorods (AuNRs) and the near-infrared (NIR) tissue absorption window. (a) The absorption of "small" AuNRs prepared by Ali *et. al.*[14] at the NIR region coincides with the (b) window where absorption of water, hemoglobin (Hb) and oxyhemoglobin (HbO_2) is minimal [15].

In synthesizing AuNRs, cetyltrimethylammonium bromide (CTAB), a cationic surfactant containing a quaternary ammonium, is generally used as stabilizing agent (**Figure 1-4**). CTAB is widely used in AuNR synthesis as a surface stabilizer as it is convenient, common, and cheap. The high concentration used results in tightly packed bilayers on AuNR surfaces, which contribute to repulsions, and consequently prevention of aggregation, stabilizing the AuNRs[16]. However, CTAB is highly toxic to cells because of its can infiltrate, damage, and create holes in the cell membrane[17,18]. Therefore, it is necessary to find an alternative, non-toxic strategy for stabilizing AuNRs in solution for translational applications. The main goal of this study was to replace CTAB in the reaction sequence with a less toxic material, and alternatively, to develop an envelope-type lipid nanoparticle with the objective of delivering the AuNRs to cancer cells.

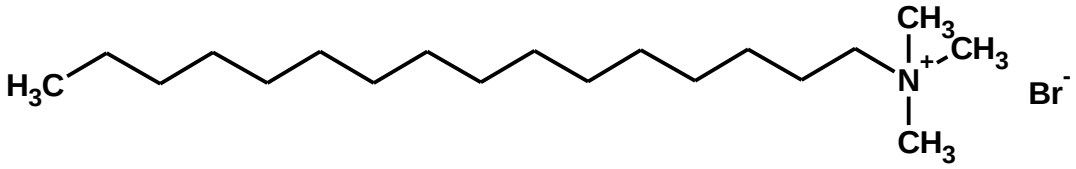

Figure 1-4. Structure of cetyltrimethylammonium bromide (CTAB).

C. Liposomes as possible carriers of gold nanorods

The surface chemistry, or the properties of the ligands present on AuNR surface, has a greater effect on cytotoxicity, both *in vitro* and *in vivo*, compared to size or aspect ratio[16]. To improve the biocompatibility of AuNRs, liposomes can be used to coat their surfaces. Liposomes are lipid-based carriers which, when administered *in vivo*, extravasate poorly into tight endothelial junctions, reducing side effects normally associated with free drugs[19], hence improving their safety profile.

Our laboratory has developed a kind of liposome which mimics envelope-type viruses (**Figure 1-5**). Envelope-type viruses, whose genomes are coated with a functionalized lipid envelope, have evolved to confer cellular targeting and the subsequent control of intracellular trafficking[20]. Inspired by this viral mechanism, multifunctional envelope-type nano device (MEND) has been used as a vehicle for plasmid DNA and other nucleic acids[21]. This structure has great advantages, in that various types of functional devices can be integrated within it, including

polyethylene glycol (PEG) to avoid clearance by the reticuloendothelial system (RES) or mononuclear phagocyte system (MPS), and targeting ligands that are designed to modify its surface[21,22].

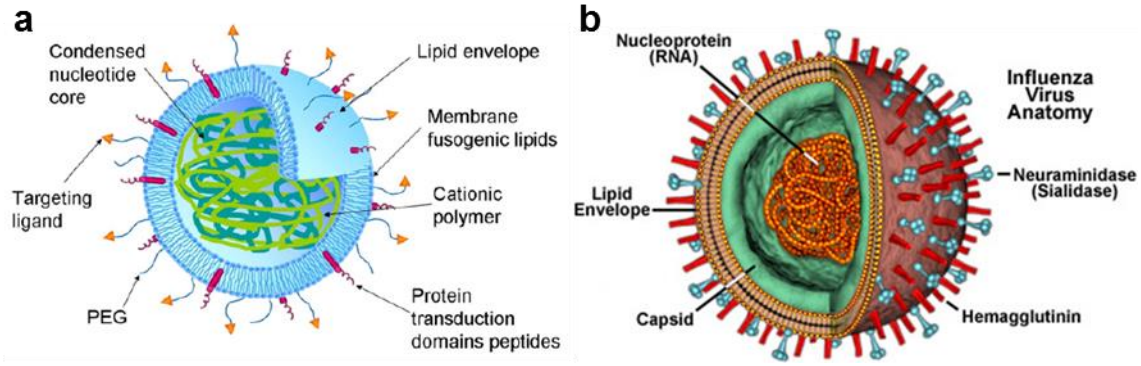

Figure 1-5. Similarities of multifunctional envelope-type nano device (MEND) and the envelope-type virus. (a) Illustration of MEND[21,23]. (b) Illustration of influenza virus [24].

Along with the functional devices, some artificial materials were developed as a component of the lipid envelope which respond to intracellular environmental triggers[25–27] like low pH. The proton sponge or pH-buffering effect involves compounds with buffering capacity and the ability to swell after protonation. During protonation, H^+ ions and water flow inside the endosome, leading to rupture of the membrane and release of the components. Tertiary amines with hydrophobic chains have this property[28].

One example of such material is SS-cleavable and Proton-Activated Lipid-like Material (ssPalm)[29], which was designed to deliver pDNA and other nucleic acids to the cytoplasm (**Figure 1-6**). Similar to lipids, the material contains two hydrophobic groups (myristic groups) that form a lipid envelope structure. The material also mounts dual sensing motifs that are responsive to intracellular environments: two tertiary amines as acidic pH-triggered positively-charged groups, and disulfide bonding as an environment-triggered reducible group [22,30]. With the aid of these functions, we assumed that the lipid particle could be efficiently taken up by cells and that the AuNRs could then be released into the cytoplasm, resulting in the promotion of photothermal effects (i.e., the induction of apoptosis and necrosis[8,31,32]).

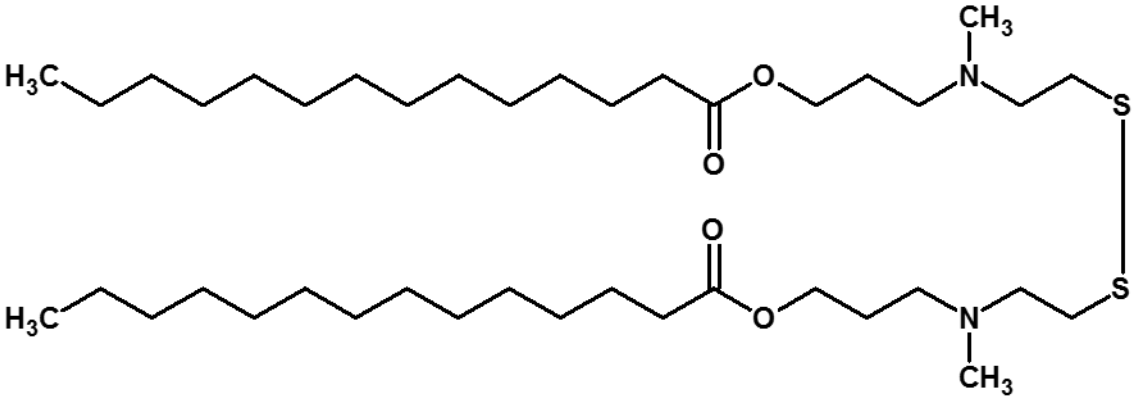

Figure 1-6. Structure of SS-cleavable and proton-activated lipid-like material-myristyl (ssPalmM).

D. Research Objectives

The overall objective of this work is to develop envelope-type lipid-coated AuNRs, and prove its applications in photothermal therapy while avoiding the non-specific toxicities associated with CTAB. The dissertation is further divided into three chapters to discuss specific parts of the nanoparticle development.

Chapter II addresses the establishment a preparation method for the nanoparticle. This includes the synthesis of AuNRs, discovery of the encapsulation method using protein, and measurement of the physicochemical properties of AuNR-MEND. Transmission electron microscopy (TEM) as a tool for verifying encapsulation is also demonstrated.

Chapter III explains the evaluation of photothermal cytotoxicity and cellular uptake of AuNR-MEND using 4T1 mouse breast cancer cells. The design and optimization of the assay is discussed, as well as the effects of various factors like irradiation power, exposure time, and nanoparticle dose and coating. Apoptosis as a mechanism of toxicity is considered. Cellular uptake is examined using fluorescence microscopy and flow cytometry.

Chapter IV provides exploratory experiments on BALB/c mice through pharmacokinetics and toxicity experiments.

The overall conclusion, implications, and possible future directions of this research work is then elaborated on in **Chapter V**.

Chapter II: Development of Lipid-Coated Gold Nanorods

A. Introduction

This chapter discusses how CTAB on the AuNR layer was replaced with several molecules leading to the development of AuNR-MEND (**Scheme 2-1**). There are several reported methods of CTAB replacement. AuNRs have previously been coated with citrate, in a two-step process involving coating with polystyrenesulfonate (PSS) as intermediate[33]. However, the use of PSS as a polymer replacement for CTAB still causes some cytotoxicity because of its negative charge[34]. Other polymers [polylysine (PLL), polyvinylpyrrolidone (PVP), starches, glycans] and smaller molecules [mercaptocarboxylic acids (MCAs)] have been used as coating too[35–37]. PEGylation is one of the most widely used methods in AuNR surface modification because it can impart a high degree of stability[38] and biocompatibility to AuNRs by the steric hindrance imparted by the long, hydrophilic PEG chains [39].

There has not been a published paper demonstrating the encapsulation of AuNRs into liposomes through transmission electron microscopy (TEM). Phospholipid-AuNR composites have been prepared before in one report, but because of the lack of TEM images as evidence, it is unclear whether this has led to encapsulation of liposomes formed by 1-palmitoyl-2-oleoyl-sn-glycero-3-phosphocholine (POPC)[40].

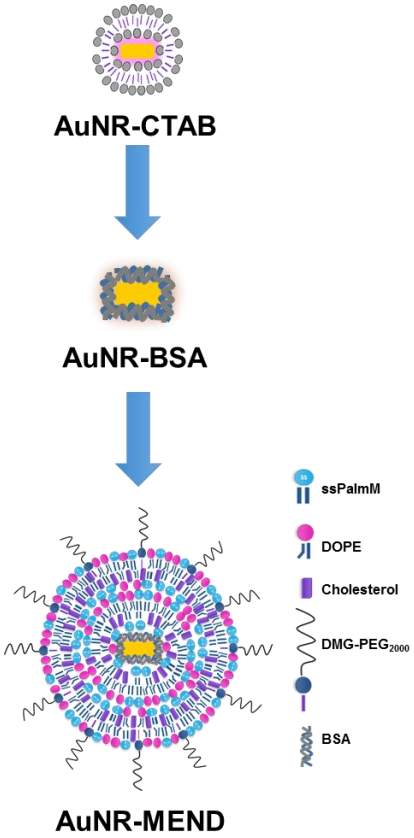

Scheme 2-1. Preparation of gold nanorod-multifunctional envelope-type nano device (AuNR-MEND).

B. Results and Discussion

1. Synthesis of "Small" Gold Nanorods

The AuNRs were synthesized using a seedless approach as described by Ali *et. al*[14]. The procedure is outlined in **Scheme 2-2**. Solutions of $HAuCl_4$, CTAB, and $AgNO_3$ were mixed. Concentrated HCl is then added to lower the pH to around 2, to lower the reducing potential of ascorbic acid[41,42]. Low pH contributes to a more controlled growth of the nanorods. When ascorbic acid is added, Au^{3+} is softly reduced to Au^{+}, changing the color of the solution from bright yellow to clear. A dilute solution of $NaBH_4$ is then injected into the solution to create seeds *in situ* by reducing Au^{+} to Au. The small seeds then serve as starting points of growth of the nanorods. After 12–18 hours, the solution turns dark purple, indicating the formation of AuNRs. It is then centrifuged and washed with deionized water to dilute CTAB to approximately 1 mM.

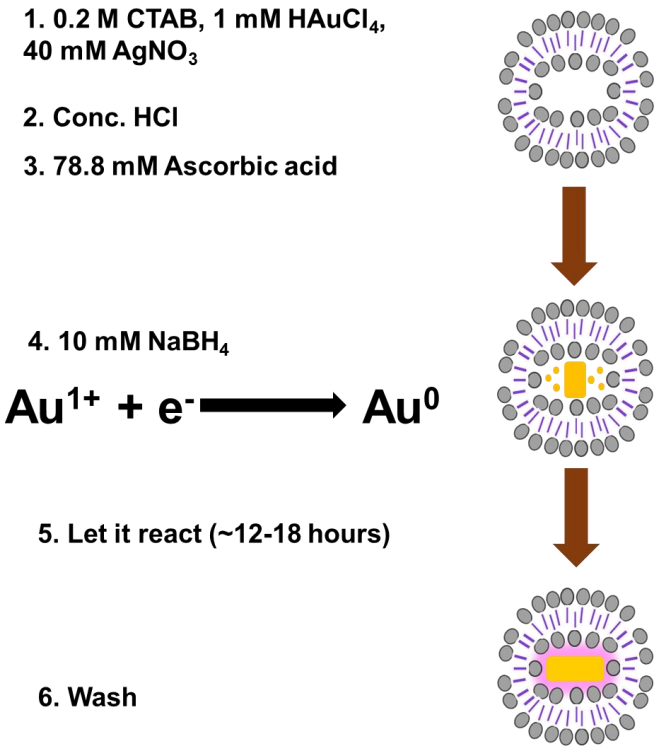

Scheme 2-2. A simplified outline of the synthesis of "Small" AuNRs using a seedless method, as adapted from Ali *et. al*[14].

The AuNRs were then observed under TEM to check its morphology and size (**Figure 2-1**). Monodisperse nanoparticles were achieved, with no evident aggregation. The dimensional data of 186 nanorods from the images was measured using ImageJ[43,36] (**Figure 2-1-c-d**). The histograms that were generated from the lengths and widths of individual particles indicate a single-peak distribution. The mean length is 29 ± 7.1 nm while the mean width is 8 ± 1.3 nm. The aspect ratio can be derived by dividing the length over the width, with the result being 3.6. Compared to 60-nm nanorods, there are less researches about "small" AuNRs. However, it was reported that 28-nm rods are more effective than longer nanorods in absorbing light and converting it to heat[44], making them better photothermal therapy agents.

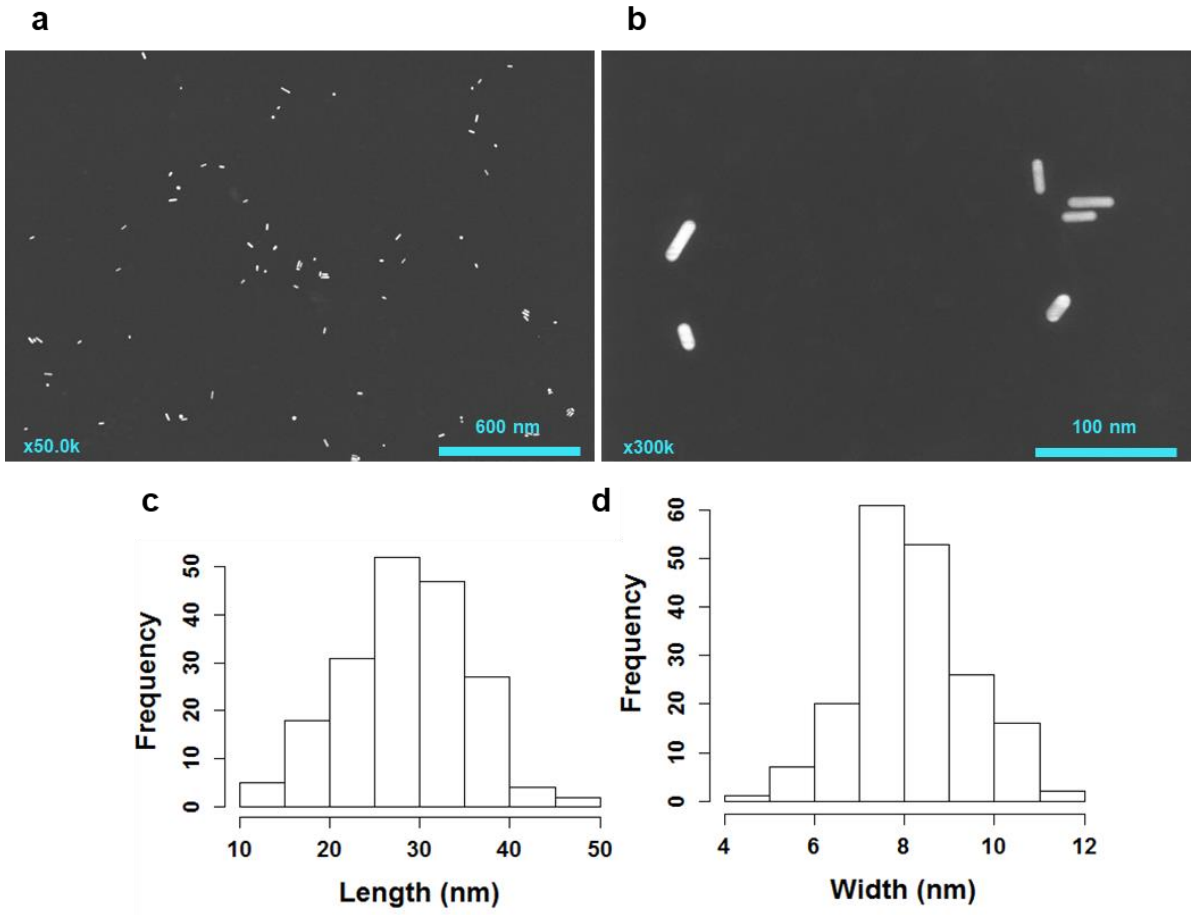

Figure 2-1. Shape and dimensions of AuNRs. (a-b) Electron microscopic images of AuNR-CTAB. (c-d) The individual length (c) and width (d) of the CTAB-stabilized AuNRs were evaluated using ImageJ, and their distributions are shown as histograms generated using R studio.

2. Discovery of the Encapsulation Method

After synthesizing the nanorods, the next step would be to encapsulate it into MEND. However, this has not always been straightforward since AuNR-CTAB could not be directly encapsulated. The original idea was that CTAB must first be removed and replaced with a ligand which is more biocompatible, prior to encapsulation into MEND. The attempts are outlined as follows:

a. Replacement of CTAB with oleate, and then encapsulation;
b. Replacement of CTAB with oleate, addition of *luc* pDNA and protamine, and then encapsulation;
c. Replacement of CTAB with oleate, addition of protamine, and then encapsulation; and,
d. Replacement of CTAB with BSA, and then encapsulation (final method).

Initial attempts to encapsulate AuNR into MEND failed until the discovery that proteins can help with the encapsulation. First, replacement of CTAB with oleate was attempted because it is a naturally-occurring fatty acid and is thus seen as less toxic than CTAB (**Scheme 2-3**). And then, after addition of plasmid DNA (pDNA) and protamine was explored, encapsulation was achieved. In the end, another biocompatible molecule, bovine serum albumin (BSA), was used as encapsulating agent. The steps leading to the eventual use of this method is briefly discussed in this part first.

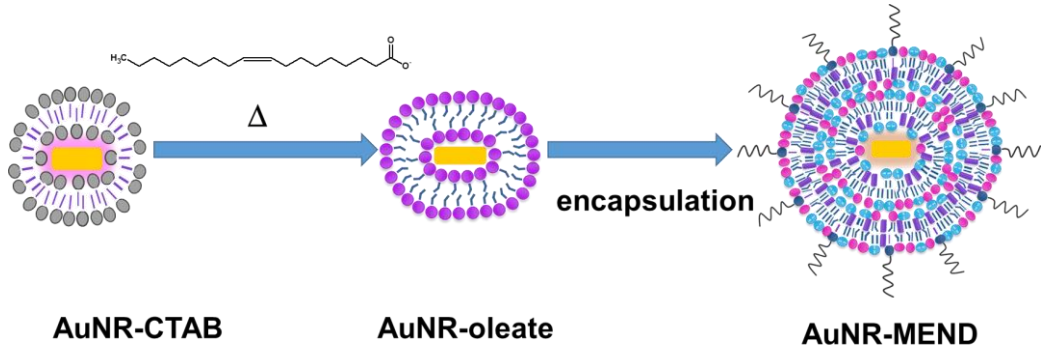

Scheme 2-3. Hypothesized scheme of AuNR-MEND preparation using oleate.

a. Replacement of CTAB with oleate, and then encapsulation

The procedure for this step was adapted from Murakami *et. al*[45]. Briefly, AuNR-CTAB was heated with a dilute solution of sodium oleate (**Scheme 2-3**). The excess oleate was then washed with water and removed by centrifugation. The AuNR-oleate suspended in buffer was then encapsulated into MEND using the alcohol dilution method (**Scheme 2-4**). In this method of liposome preparation, the lipid mixture is dissolved in ethanol. The alcoholic solution is then rapidly diluted with a buffer solution containing the cargo. This lowers the lipid concentration beyond their critical micelle concentration (CMC), forming liposomes. The organic solvent is then washed with buffer through centrifugal filtration[29,46].

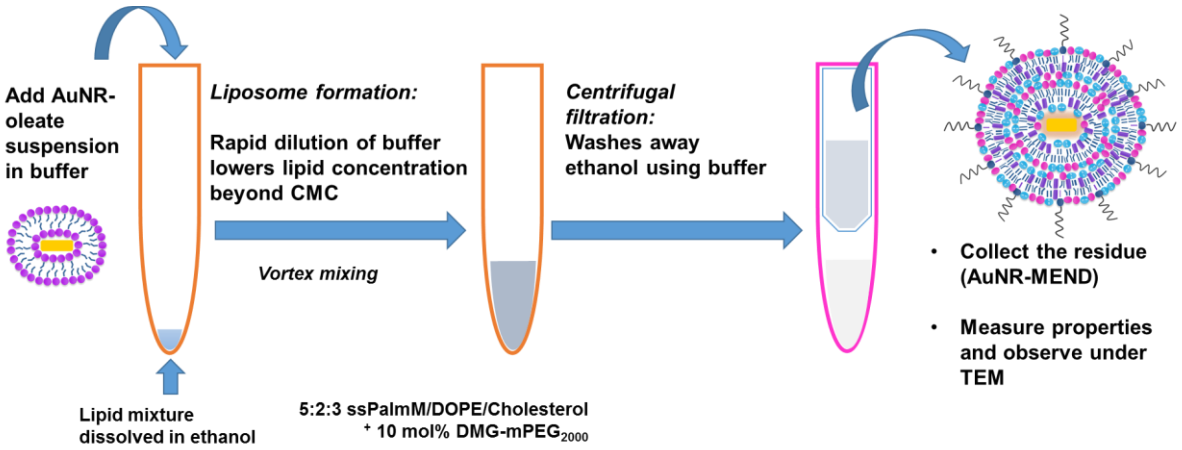

Scheme 2-4. Brief illustration of AuNR-MEND preparation using the alcohol dilution method.

However, when the resulting nanoparticle was viewed under TEM, no encapsulation was observed (**Figure 2-2**). Instead, AuNRs adsorbed on the surface of liposomes. It is possible that oleate simply mixed with the other lipids to form liposomes, leaving the nanorods unencapsulated but still attached to the lipids. This type of nanoparticles have been previously reported as Liposome-AuNR hybrids and has been used to deliver siRNA into cells through a heat-triggered response[47,48].

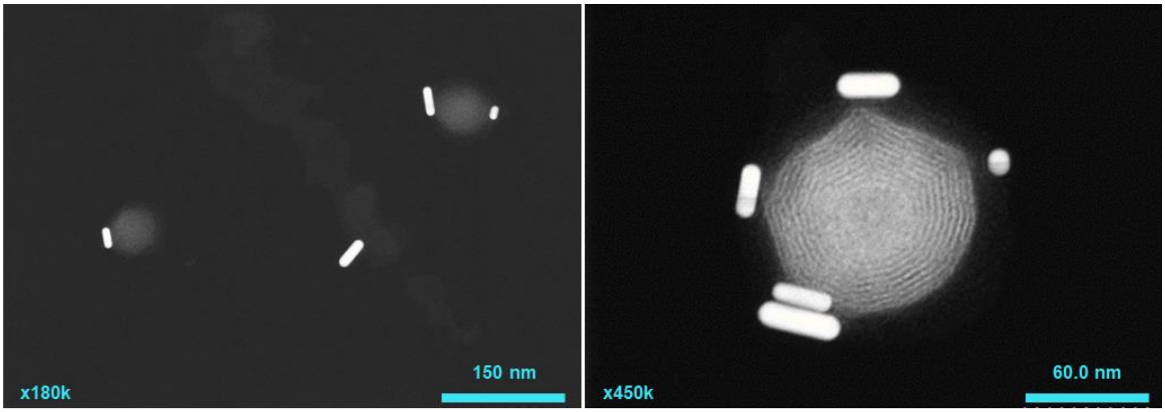

Figure 2-2. Electron microscopic images of AuNR-oleate adsorbed on liposome surfaces.

b. Replacement of CTAB with oleate, addition of *luc* pDNA and protamine, and then encapsulation

The unexpected similarity of the produced nanoparticles to the previous reports [47,48] led to the exploration of its possible use in heat-triggered gene delivery. A core particle of *luc* pDNA condensed with protamine was then mixed with

AuNR-oleate prior to liposome preparation (**Scheme 2-5**). The expectation was that pDNA would be encapsulated inside the liposome-AuNR hybrid. Surprisingly, the nanoparticles observed showed that multiple AuNRs were encapsulated inside liposomes (**Figure 2-3**).

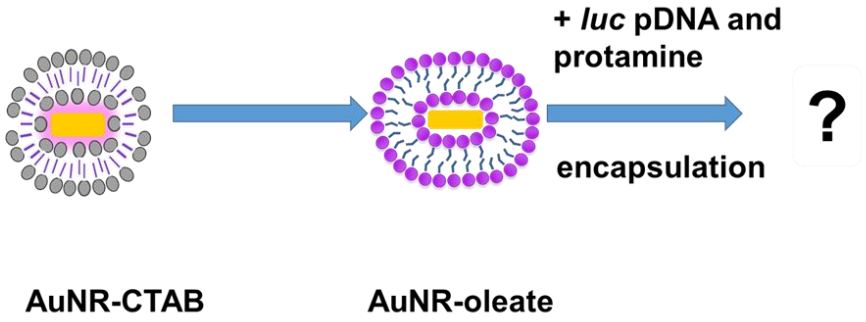

Scheme 2-5. Hypothesized scheme of AuNR-MEND preparation using oleate, *luc* pDNA, and protamine.

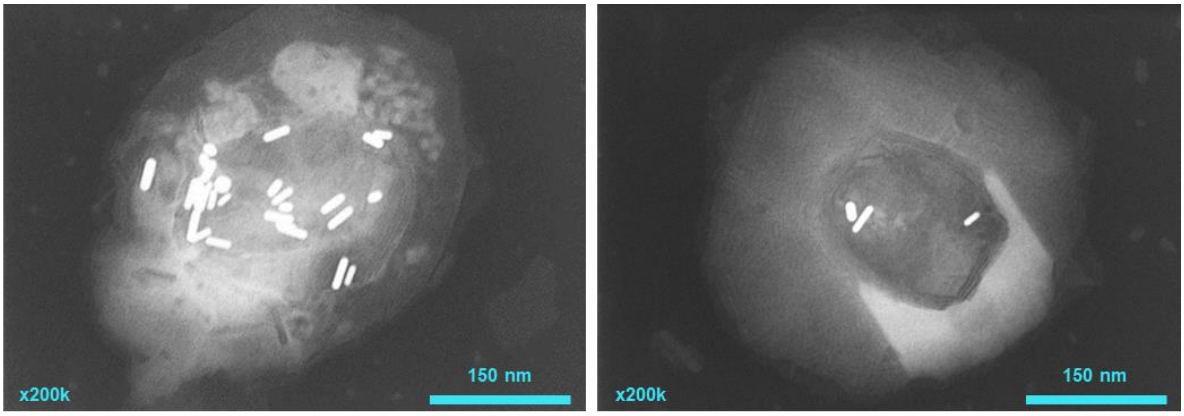

Figure 2-3. Electron microscopic images of multiple AuNRs encapsulated in a liposome with the aid of *luc* pDNA and protamine.

This meant that either the pDNA or the protamine was the driving force for encapsulation. Plasmid DNA is a large biomolecule by nature, which needs to be condensed with protamine prior to encapsulation. Hence, it is unlikely that this could have caused the encapsulation of AuNRs. Protamine was the more probable cause of encapsulation. The attempt to encapsulate pDNA with liposome-AuNR hybrids was then abandoned and the lead with protamine was pursued.

c. Replacement of CTAB with oleate, addition of protamine, and then encapsulation

In the third attempt, only protamine was added to AuNR-oleate prior to liposome preparation (**Scheme 2-6**). Judging from the TEM images (**Figure 2-4**), AuNRs were clearly inside the liposomes, confirming the hypothesis that it was the cause of encapsulation. The images also show single nanorods inside the lipid structure.

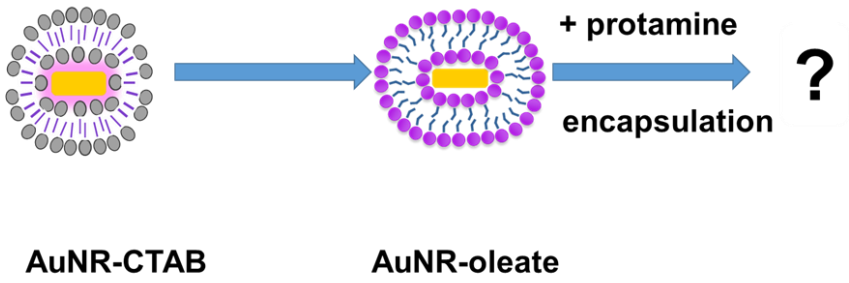

Scheme 2-6. Hypothesized scheme of AuNR-MEND preparation using oleate and protamine.

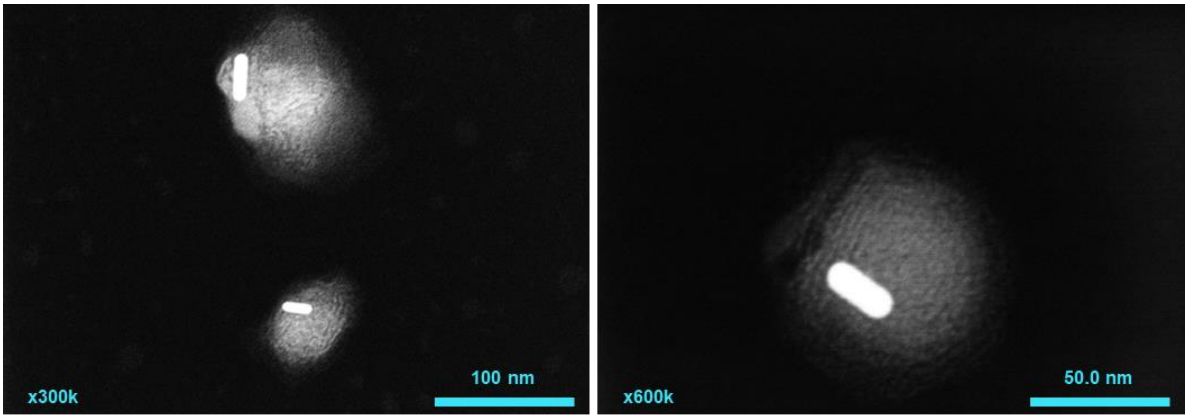

Figure 2-4. Electron microscopic images of AuNR-oleate-protamine-MEND.

Protamine is an arginine-rich (70%) protein, making it basic[49]. It also has cysteine residues which can be used to interact with DNA[50]. Both features can help explain its interaction with AuNR-oleate. At acidic and neutral pH, protamine would be cationic; hence, it would interact with the oleate lipid layer through electrostatic forces. It is also possible that the –SH group in the cysteine residues could form a coordinate bond with the Au in the AuNR surface. Aside from these features of protamine, AuNR-oleate can successfully fuse with low-density

lipoprotein (LDL)[45]. While there are no in-depth studies of AuNR-protamine interaction, the above statements could explain the encapsulation of AuNR-oleate inside the liposomes using protamine.

d. Replacement of CTAB with BSA, and then encapsulation

Even if the encapsulation of AuNR inside liposomes was successful using protamine, some problems were identified in this procedure. First, the preparation of AuNR-oleate resulted to diluted AuNRs. The concentration was often already low prior to encapsulation with MEND. When repeatedly washed, the nanoparticles tended to aggregate. Second, as mentioned already, AuNR-protamine interactions are less studied, compared to other proteins like BSA. It has been reported that RNA, protamine, and Au nanospheres show some interaction[51] but it is unknown whether this data to can be extended to protamine-AuNR interactions since the spheres and rods also have different surface chemistry. On the other hand, BSA is a known suspending agent and has been reported to stabilize AuNRs over a wide range of temperature and pH[52]. AuNR-BSA can also be prepared in high concentrations [~optical density (OD) 30] without aggregation (**Figure 2-5**), which is ideal for MEND preparation. The replacement of CTAB with BSA is illustrated in **Scheme 2-7**. BSA can strongly interact with AuNRs through the –SH group in its cysteine residues[53] but hydrophobic interactions are said to dominate BSA-AuNR interactions[54]. Electrostatic interactions were also reported to play a role[55]. It has been proven through Surface-Enhanced Resonance Spectroscopy (SERS) that BSA completely replaces CTAB from the AuNR surface through the process described below[52].

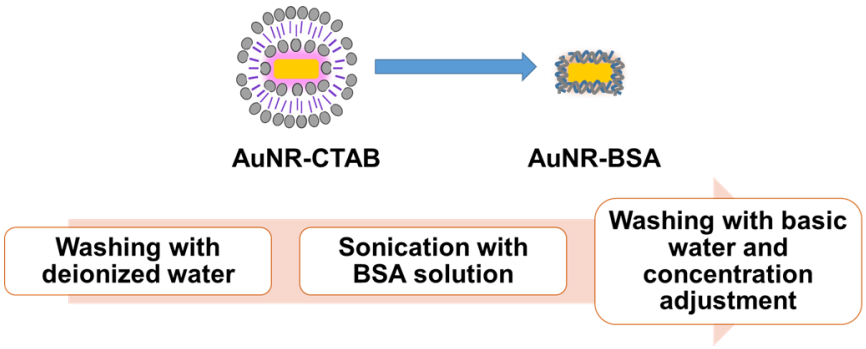

Scheme 2-7. Brief illustration of CTAB replacement by BSA to form AuNR-BSA.

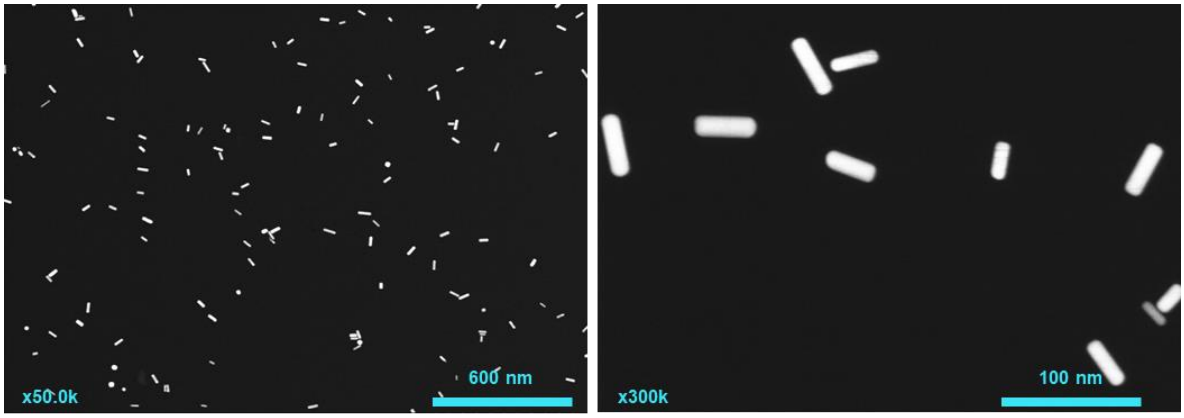

Figure 2-5. Electron microscopic images of AuNR-BSA.

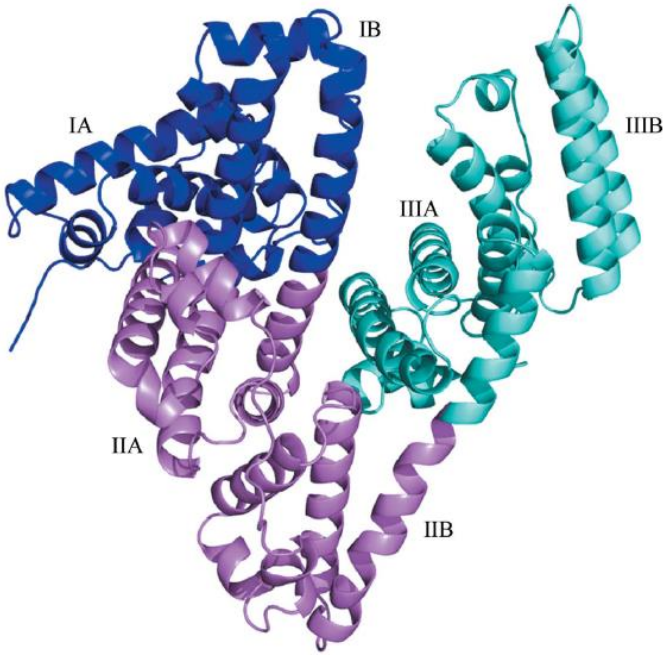

Figure 2-6. Structure of bovine serum albumin (BSA) from Bujacz *et. al.*[56].

After coating the particles with BSA, they were then encapsulated into MEND using the alcohol dilution method as described above. TEM images confirmed that the AuNRs were encapsulated inside the lipid structures (**Figure 2-7-a-b**). During this process, the lipids could have possibly spontaneously formed vesicles through electrostatic interactions with the negatively charged AuNR-BSA and the positively charged ssPalmM. BSA has several hydrophobic pockets in its subunits: FA1 in subunit IB, FA3 and FA4 in subunit IIIA, and FA7 in subunit IIA (**Figure 2-6**)[56]. These hydrophobic pockets could have interacted with the lipids[57] in MEND resulting in the encapsulation of AuNR-BSA. This is the first report of encapsulation of AuNRs into liposomes using protein.

However, encapsulation of proteins in liposomes are possible and the same driving forces could have contributed to AuNR-MEND formation. Components like cholesterol have been reported to be important in enhancing encapsulation of proteins into liposomes[58].

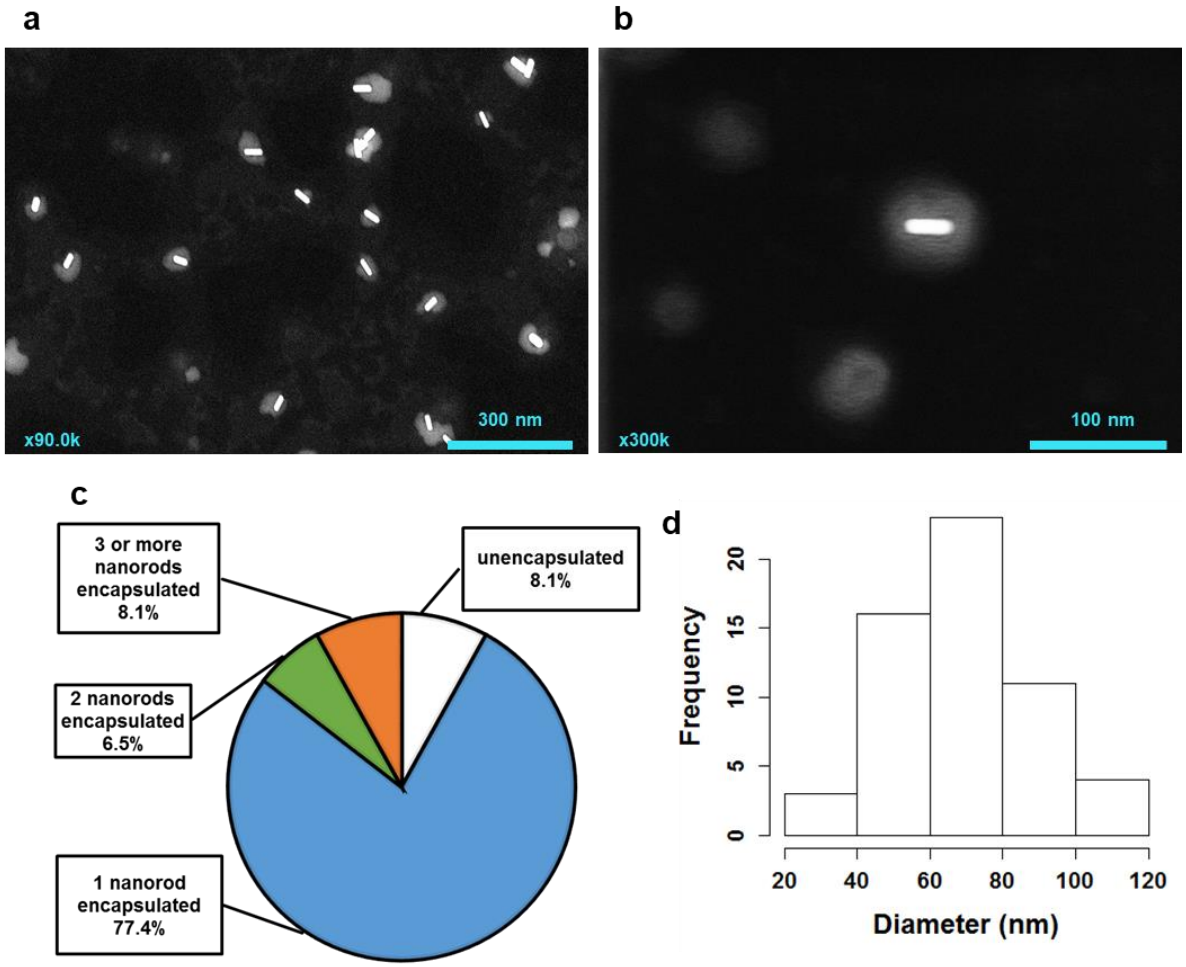

Figure 2-7. Electron microscopic images, and encapsulation and size data of AuNR-MEND. (a-b) TEM images of the AuNR-MEND, prepared by coating the AuNRs with BSA prior to encapsulation in the MEND. The lipid layer was stained with 1% phosphotungstic acid. (c) Percentage of encapsulated and unencapsulated nanoparticles obtained by manual counting (n = 62). (d) The individual diameter of AuNR-MEND was evaluated using the ImageJ software, and its distribution is shown as a histogram.

As previously observed with protamine, single nanorods were found inside liposomes. However, some liposomes contain more than one nanorod, and some nanorods are not encapsulated at all. From the TEM images, a total of 62 nanostructures were then counted and classified into “unencapsulated”, “1 nanorod encapsulated”, “2 nanorods encapsulated”, or “3 or more nanorods encapsulated” (**Figure 2-7-c**). The % encapsulation was then calculated, showing that a total of 91.9% of the nanorods were encapsulated. However, only 77.4% contained single nanorods inside the liposomes. The average diameter of the spherical AuNR-MEND particles was also measured using ImageJ (**Figure 2-7-d**). A single distribution peak can be derived from its histogram, with the average diameter being 68 ± 18.3 nm.

3. *Physicochemical characteristics of AuNRs*

It is important to monitor the change of physicochemical properties of AuNR throughout the preparation. The UV-Vis-NIR spectrum, together with TEM, gives important clues on the aggregation level of AuNRs[41]. The absorbance at ~800 nm [Longitudinal Surface Plasmon Resonance (LSPR) peak] is also an essential property to maintain, since the photothermal effect will be lost if this peak is diminished. **Figure 2-8-a** shows that the LSPR peak shifted slightly to a longer wavelength during the preparation. This is indicative of a change of refractive index on the AuNR surface[35].

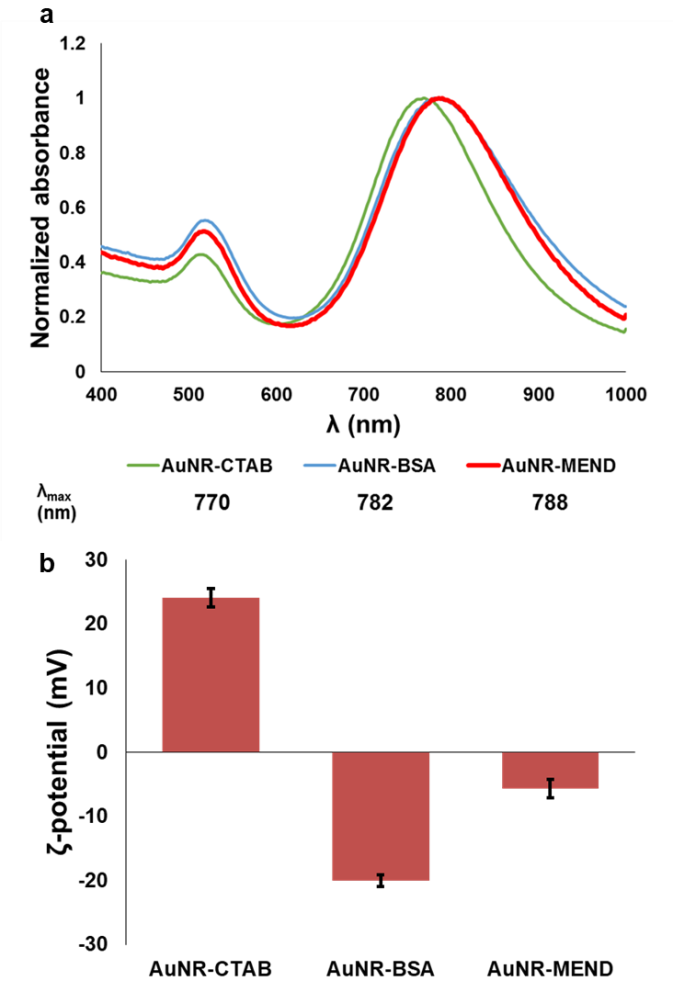

Figure 2-8. Physicochemical properties of AuNR preparations. (a) Normalized NIR absorbance profiles and (b) ζ -potentials of AuNR-CTAB, AuNR-BSA, and AuNR-MEND. Error bars represent ± S.D. for three different experiments performed in triplicate.

The ζ-potential is a measure of the surface charge of a particle. The original CTAB-stabilized AuNRs were positively charged, since CTAB contains a quaternary ammonium group. The replacement of CTAB as the coating material with BSA then resulted in a drastic inversion in the ζ-potential from +24 ± 1.4 to -20 ± 1.0 mV (**Figure 2-8-b**). Since the isoelectric point (pI) of BSA is 4.7, it is largely negative at pH 7.4[59]. After encapsulation into MEND, the ζ-potential became nearly neutral (-5.7 ± 1.44 mV). This is important for nanoparticle biocompatibility.

The hydrodynamic diameter was noticeably larger than the TEM-based diameter (**Figure 2-7-d**) since this includes the water molecules adsorbed on the hydrophilic surface of AuNR-MEND. The size profile showed a homogenous distribution with a single peak at 92 ± 4.4 nm, indicating that it was monodisperse and overall spherical (**Figure 2-9**). When the hydrodynamic size profiles of AuNR-CTAB and AuNR-BSA were measured, many peaks were observed, including those appearing at >10 nm (**Figure S-1**), which is due to the rotational diffusion exhibited by non-spherical particles[34,60].

This size is also ideal for biological applications, being less than 200 nm[19]. This is tackled in greater detail in Chapter IV.

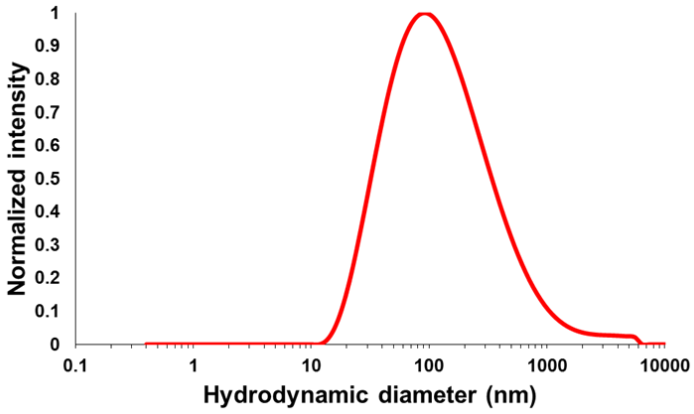

Figure 2-9. Size distribution of AuNR-MEND evaluated by dynamic light scattering (DLS).

4. Measurement of AuNR-BSA concentration

To convert the OD of AuNRs to Au concentrations, solutions of AuNR-BSA were analyzed by inductively coupled plasma-atomic emission spectroscopy (ICP-AES). This was performed to know the exact Au concentrations used in the proceeding biological assays. OD at λ_{max} is shown to be predict AuNR concentration in a linear manner from OD 0 to 1 (**Figure 2-10**).

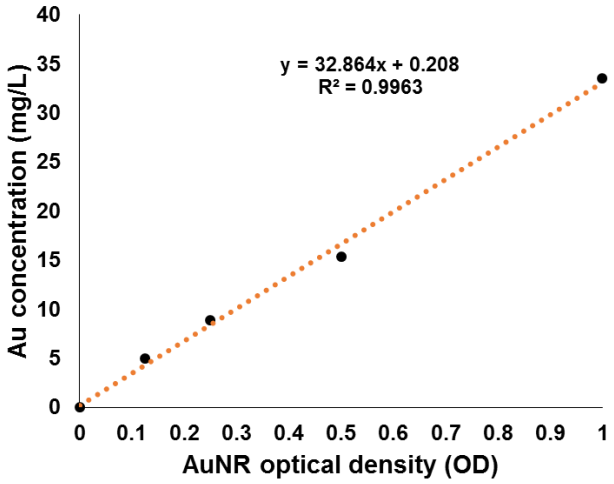

Figure 2-10. Relationship AuNR optical density with Au concentration in mg/L as measured using inductively-coupled plasma atomic emission spectroscopy (ICP-AES).

C. Conclusion

AuNRs were synthesized by the seedless method and yielded monodisperse nanoparticles with 29 nm x 8 nm dimensions. It was discovered that elimination of CTAB and encapsulation into MEND was not straightforward but was finally achieved with the addition of protein. NIR absorption was maintained throughout the encapsulation method, while the ζ-potential changed, and turned neutral after the final step. The hydrodynamic diameter of AuNR-MEND was 92 nm. From the TEM images and physicochemical properties, it can be concluded that the preparation method was established and that AuNR-MEND was ready to be tested for biological applications.

D. Experimental Section

1. AuNR Synthesis

$HAuCl_4$ (cat. # 520918-1G), $NaBH_4$ (cat. # 213462-25G), $AgNO_3$ (cat. # S6506-5G), CTAB (cat. # H5882-100G), ascorbic acid (cat. # A92902-25G), and BSA (cat. # A6003-25G) were purchased from Sigma-Aldrich. Hydrochloric acid (cat. # 080-01006) were purchased from Wako. AuNRs were prepared by seedless synthesis following the method of Ali *et. al.*, with some modifications[14]. The growth solution was prepared at 25–30 °C in a 500-mL plastic bottle. CTAB (200.0 mL, 0.2 M) was added to 200.0 mL of $HAuCl_4$ (1.0 mM). $AgNO_3$ (10.8 mL, 4.0 mM) was then added, after which the bottle was inverted once to gently mix the reagents. HCl (320.0 µL, 37%) was then added to the solution to lower the pH to around 2. Afterwards, ascorbic acid (280 µL, 78.8 mM) was added to the solution. The tube was then gently inverted multiple times until the solution became clear. Ice-cold $NaBH_4$ (600 µL, 10 mM) was immediately injected to the growth solution, resulting in a slow change in color to purple. The reaction was then placed in an incubator (maximum 30 °C) and allowed to react overnight. The solutions were centrifuged for 15 min at 14,500 rpm, and the supernatant was removed. The precipitate was resuspended in water and spun down under the same centrifugation conditions. The supernatant was again removed and then resuspended in 1 mM CTAB.

2. Stabilization of AuNRs by BSA

Stabilization with BSA was carried out according to the procedure by Tebbe *et. al.*[52], with minor modifications. The AuNRs in 1 mM CTAB from the previous step were slowly added to a solution of BSA solution (10 mg/mL) in 0.02% citrate (pH 7.4) under ultrasonication (Branson Digital Sonifier-250, Danbury, CT) in a 1:1 v/v ratio. The mixture was then further sonicated for 30 min in a bath sonicator (Aiwa AU-25C, Aiwa Co., Tokyo) and then centrifuged (10,000 rpm, 15 min). The pellet was then resuspended in a 10 x diluted BSA solution (1 mg/mL BSA, 0.02% citrate, pH 12), and then stirred for at least 24 h at 4 °C. The solution was then centrifuged

(10,000 rpm, 15 min), and the pellets were then resuspended in water (pH 11–12) to achieve the desired concentration (~ OD 30).

3. Preparation of MEND

MEND was prepared using the alcohol dilution method[29,30]. AuNR-BSA was encapsulated into a lipid envelope with a composition of ssPalmM:DOPE:cholesterol (5:2:3 molar ratio) plus 10 mol% of DMG-mPEG$_{2000}$. The lipids (500 nmol total) were dissolved in 100 µL of ethanol, and then rapidly diluted with 130 µL of AuNR-BSA solution (OD 30) in 420 µL malate buffer (20 mM, pH 4). The solution was then further diluted to approximately 5% v/v ethanol by immediately adding malate buffer (20 mM, pH 4). The diluted nanoparticle preparation was afterwards filtered and concentrated by centrifugation using an Amicon Ultra 4 (Millipore) ultrafilter (1,000 g, 15 min, 30 °C). The remaining suspension on the upper column was resuspended in PBS (pH 7.4), and again centrifuged using the same conditions. The AuNR-MEND concentration was then measured using UV-Vis-NIR spectroscopy (Beckman Coulter DU 730) and expressed in optical density (OD) at wavelength of maximum absorbance (~800 nm).

4. Physicochemical characterization

The diameter and ζ-potential of the nanoparticles were determined using an electrophoretic light-scattering spectrophotometer (Zetasizer, Malvern Instruments Ltd.). For TEM observations, the nanoparticle suspensions were mounted on a copper grid (Cat. No. 6511, Nisshin EM Co. Ltd., Tokyo), lipids were stained with 1% phosphotungstic acid, and then dried overnight prior to being observed using a Hitachi HD2000 scanning transmission electron microscope with a voltage of 200kV. The average length and width of individual AuNRs as well as the diameter of AuNR-MENDs in TEM were measured by ImageJ software[43]. The histograms were then generated using RStudio. Encapsulated and unencapsulated AuNRs were counted to estimate % encapsulation.

5. Measurement of Au concentration by ICP-AES

The Au concentration was measured using inductively coupled plasma atomic emission spectroscopy (ICP-AES). AuNR-BSA solutions with known OD was desiccated overnight and digested with aqua regia (1 mL) at 80 ºC for 10 h to enable complete ionization of Au. The solutions were diluted with 10 mL of deionized water and subjected to spectroscopic analysis[61]. A calibration curve for Au^{3+} at various concentrations was made using a commercial standard[62].

Chapter III: Evaluation of Photothermal Cytotoxicity and Cellular Uptake

A. Introduction

The working hypothesis in this doctoral work is that AuNR-MEND is taken up by the cell through endocytosis and then once inside, NIR irradiation can be used. The nanoparticles then absorb NIR light and convert it to heat, damaging intracellular components, and eventually killing the cell (**Figure 3-1**). It is possible that cell death may be initiated by apoptosis, a process of controlled cell death, where the cell is demolished from within, minimizing damage to neighboring cells[63]. This chapter examines the photothermal cytotoxicity and cellular uptake of AuNR-MEND and other nanoparticles on 4T1 mouse breast cancer cells.

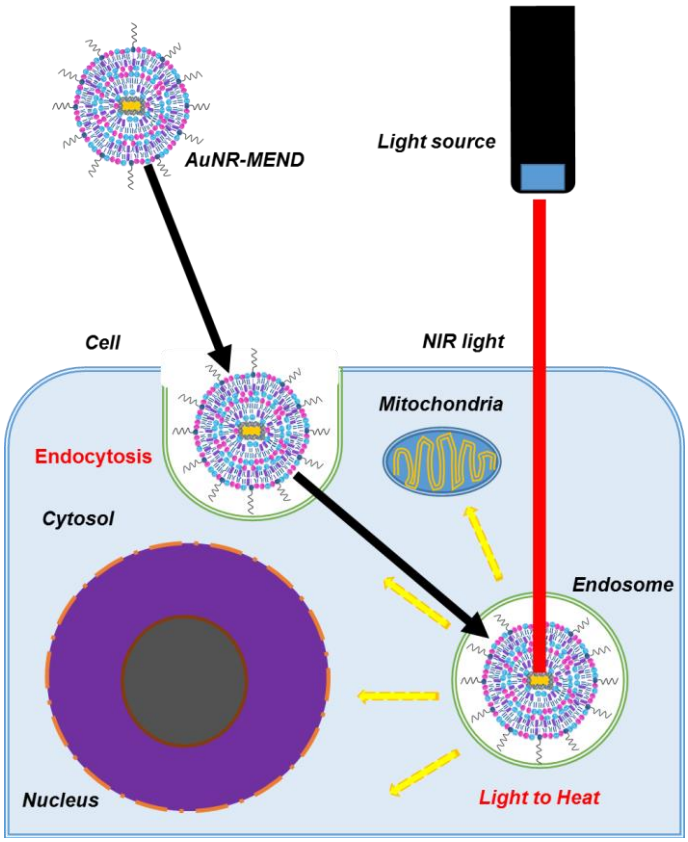

Figure 3-1. Proposed mechanism for cell damage: AuNR-MEND is taken up by the cells, and subsequently generate heat in response to the NIR irradiation, consequently killing the cells.

B. Results and Discussion

1. Design of photothermal cytotoxicity assay

Photothermal cytotoxicity requires measurement of cell survival after NIR irradiation. The assay set-up (**Figure 3-2**) requires an NIR source, for which, a xenon (Xe) lamp is used. The Xe lamp provides a continuous light source from 750–900nm, with the beam concentrating on a 1 x 1 cm^2 spot, enough to cover one well at a time in a 96-well assay plate. The irradiation treatment involved placing the lamp 7 cm over the plate which is then placed on top of a slide warmer. The slide warmer fixes the baseline temperature at 37 ºC, thereby maintaining this temperature for all the other cells in the plate during irradiation. Irradiation is expected to raise the temperature of the medium, which was measured using a probe thermometer.

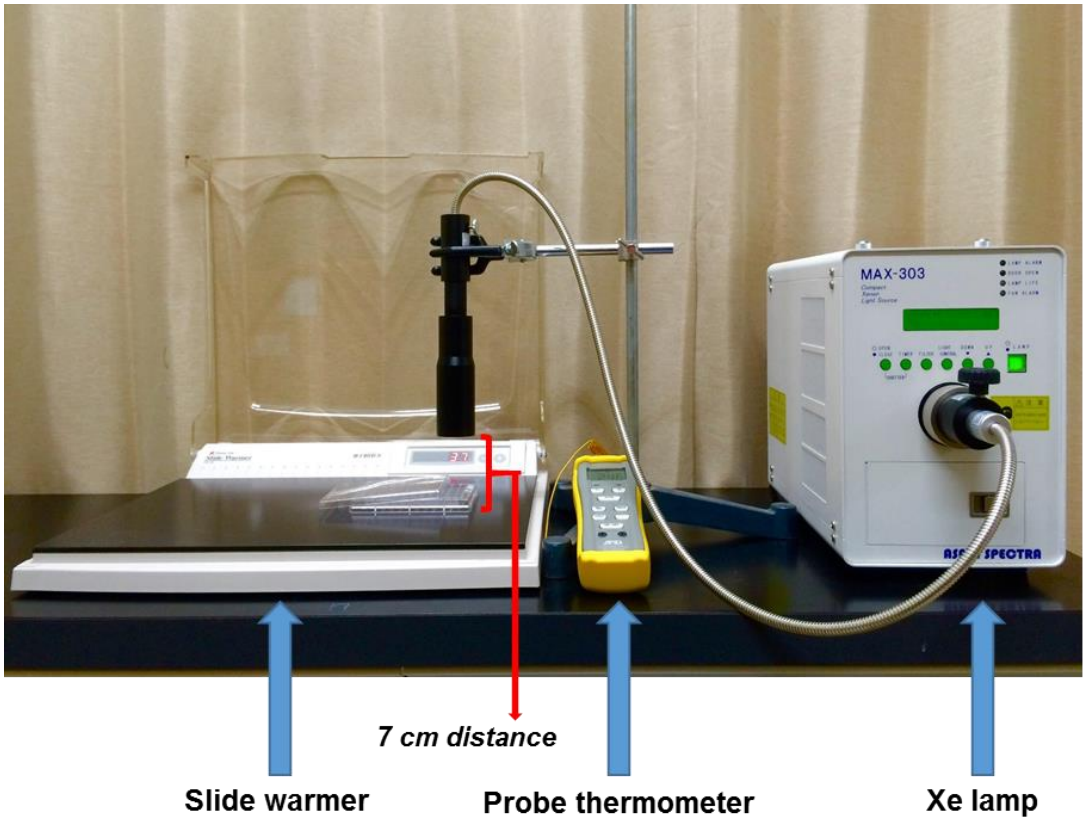

Figure 3-2. Set-up of photothermal cytotoxicity irradiation.

WST-8 assay, which is based on the NAD^+ to NADH reduction of living cells, was chosen as a simpler and more sensitive alternative to the MTT assay[64].

Assessment of photothermal cytotoxicity was performed four hours after irradiation (**Scheme 3-1**).

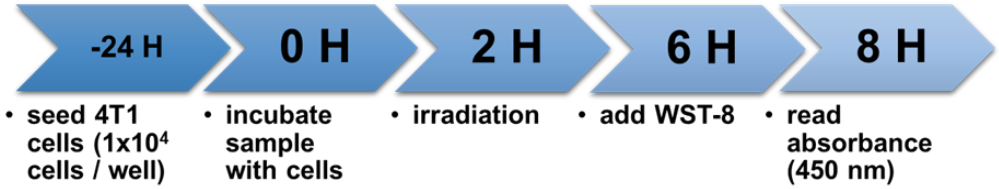

Scheme 3-1. Outline of photothermal cytotoxicity assay.

2. Optimization of irradiation power and time

The AuNR-MEND concentration was primarily fixed at OD 0.5 or 16.4 mg Au/L while the assay was optimized in terms of irradiation power and time. It was found that while the irradiation power between 0.5 W/cm^2 and 1.0 W/cm^2 does not affect cytotoxicity, the irradiation time does. More than 80% of the cells were killed within ~ 6 min of irradiation, regardless of the light power (**Figure 3-3-a**). In this experiment, the temperature of the medium was increased to ~40 °C and ~56 °C after 6 min of irradiation with a light power of 0.5 W/cm^2 vs 1.0 W/cm^2, respectively (**Figure 3-3-b**). These results clearly showed that AuNR-MEND possesses photothermal activity.

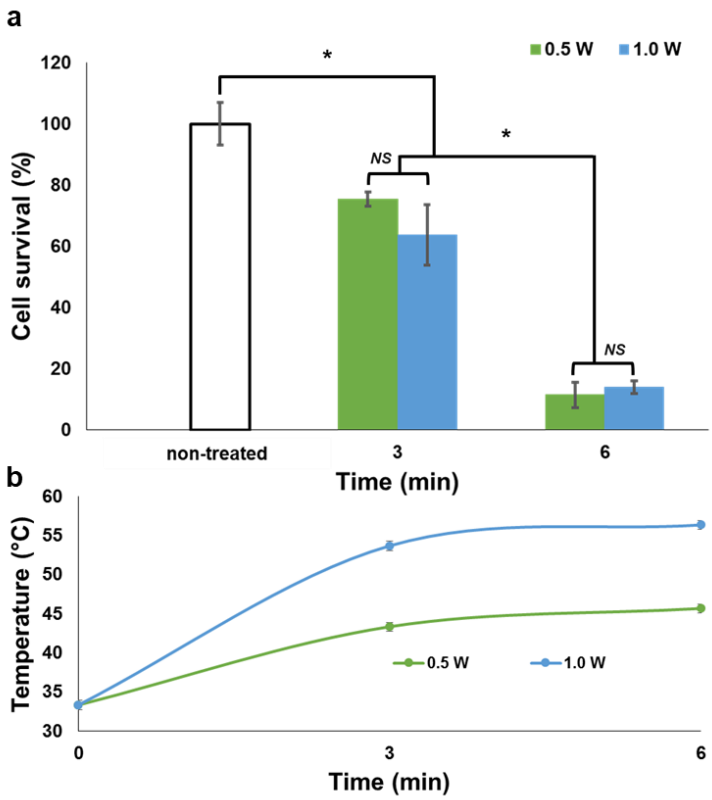

Figure 3-3. Optimization of photothermal cytotoxicity assay. (a) Evaluation of cell viability and (b) medium temperature after NIR irradiation for 0, 3, and 6 minutes using 0.5 and 1.0 W light power. Error bars represent ± S.D. for three different experiments performed in triplicate (**p<0.05, One-way ANOVA, Tukey's HSD)*.

The irradiation power and time for the rest of the assays were then fixed at 0.5 W/cm^2 and 6 min, respectively. To check the effect of external medium temperature rise on cells, the heating effect was emulated by exposing the cells to 60 °C-pre-warmed medium (**Scheme 3-2**). Most surprisingly, the 6 min incubation of the cells in pre-warmed medium showed marginal cytotoxicity (at most 25%) (**Figure 3-4**). Thus, the strong cytotoxic effect produced by the AuNR-MEND cannot simply be explained from the point of view of extracellular temperature. It is then postulated that the photothermal cytotoxicity of the AuNRs is largely caused by heat produced inside the cells.

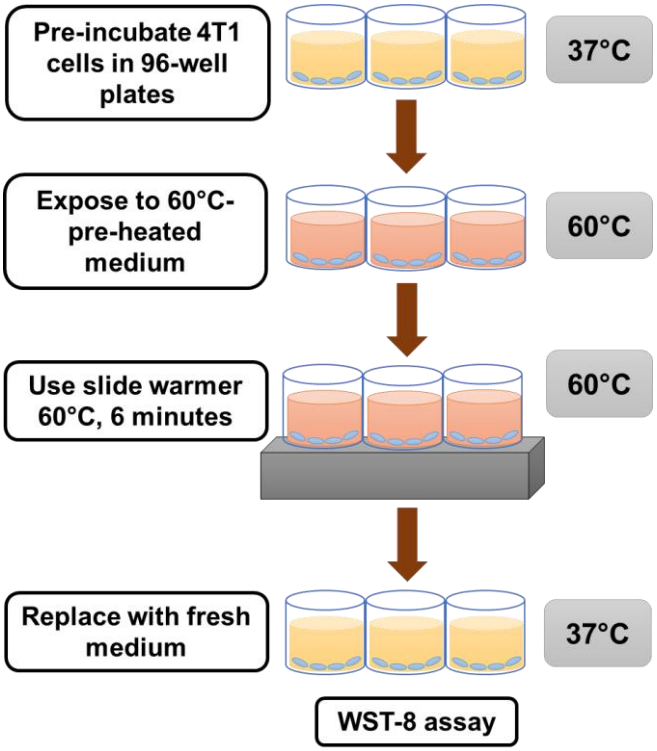

Scheme 3-2. Procedure of evaluation of cell viability after a 6 min exposure to pre-heated medium at 60 °C.

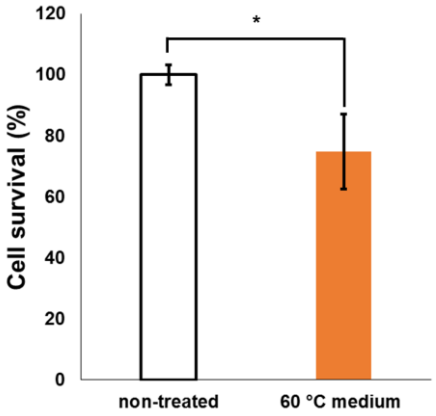

Figure 3-4. Evaluation of cell viability after a 6 min exposure to pre-heated medium at 60°C. Error bars represent ± S.D. for three different experiments performed in triplicate (* *p<0.05, Unpaired t-test*).

3. Determination of effect of coating and dose variation

The photothermal cytotoxicity of the previous formulations was then compared with that of AuNR-MEND. While irradiation with or without any AuNR sample causes slight toxicity (15–28% cell death), it was observed that only AuNR-BSA and AuNR-MEND exhibit significant photothermal cell-killing effect (**Figure 3-5**). This further

supported the decision to choose the development of AuNR-MEND using BSA rather than protamine, aside from the advantages discussed in Chapter II. It is possible that because of the excess oleate, formation of protein corona around AuNR-oleate and AuNR-oleate-protamine-MEND could have occurred, increasing their overall hydrodynamic size and lowering cell uptake, thus diminishing their photothermal cytotoxicity[65].

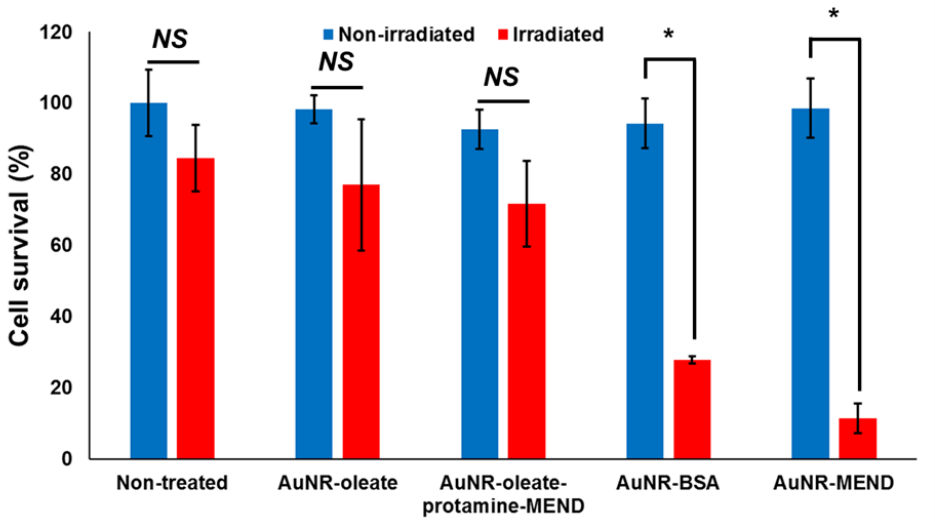

Figure 3-5. Evaluation of photothermal cytotoxicity of different AuNR preparations: AuNR-oleate, AuNR-oleate-protamine-MEND, AuNR-BSA, and AuNR-MEND without and with irradiation at 0.5 W/cm^2 for 6 min. Error bars represent ± S.D. for three different experiments performed in triplicate (**p<0.05, Unpaired t-test)*.

The dose-dependent cytotoxic effects of AuNR-CTAB, AuNR-BSA, and AuNR-MEND with or without NIR irradiation for 6 min at 0.5 W/cm^2, were then studied. The doses used were 4.1 to 32.9 mg Au/L (OD 0.125 to 1.0). AuNR-CTAB showed drastic cytotoxicity in both the presence and absence of NIR irradiation, even at low concentrations. This indicates that traces of CTAB remaining in the sample caused non-specific cytotoxicity, supporting the hypothesis that the original AuNR-CTAB is not appropriate for translational applications (**Figure 3-6**). Confocal laser scanning microscopy (CLSM) images show that AuNR-CTAB-treated cells have a morphology different from live cells, since they are detached from the plate

(**Figure S-2**). In contrast, the AuNR-BSA and AuNR-MEND showed little or no cytotoxic effects in the absence of NIR irradiation, as was previously shown in Figure 3-5, indicating that these particles are intrinsically compatible for *in vivo* applications.

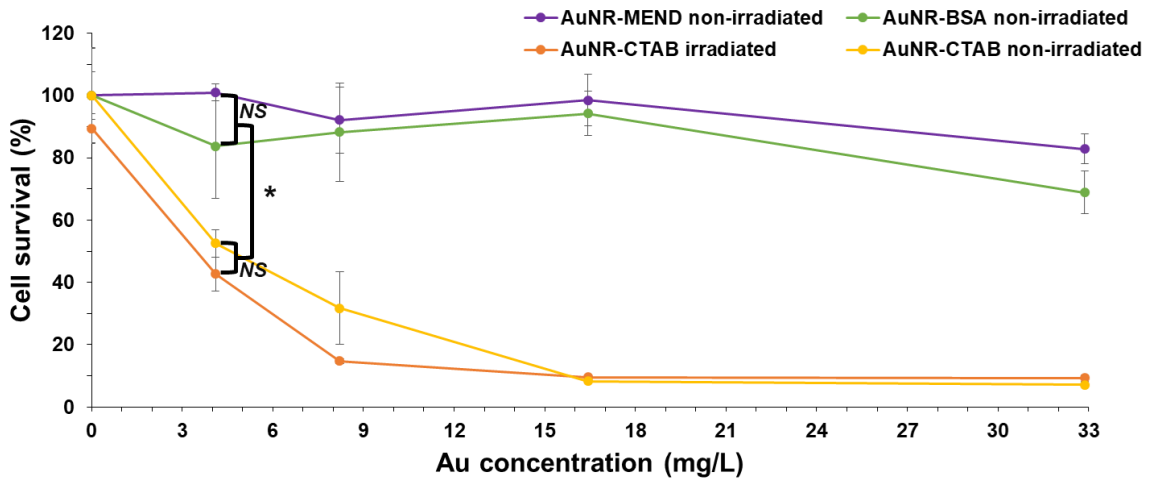

Figure 3-6. Dose-response curves for the cytotoxicity of AuNR-MEND, AuNR-BSA, and AuNR-CTAB without NIR irradiation and for AuNR-CTAB with irradiation at 0.5 W/cm^2 for 6 min. Error bars represent ± S.D. for three different experiments performed in triplicate (*$p<0.05$, *One-way ANOVA, Tukey's HSD)*.

Under NIR irradiation, both particles exhibited cytotoxic effects (**Figure 3-7**). In these comparisons, the maximum cytotoxicity was 75% in AuNR-BSA, even at a higher dose (32.9 mg/L), while it exhibited a higher cytotoxicity at a smaller dose (4.1 mg/L) in comparison with AuNR-MEND. AuNR-MEND conferred almost complete cytotoxicity at a higher doses (16.4–32.9 mg/L). It is possible that AuNR-BSA showed heterogeneous uptake, although this is still currently being investigated. If its uptake is not uniform, then AuNR-BSA will probably produce varying responses according to dose. It was postulated that AuNR-MEND uptake is more efficient and uniform, hence the shape of its dose-response curve. The dose-temperature increase relationship for both nanoparticles are both linear and comparable, hence temperature increase alone cannot explain the difference in cytotoxicity (**Figure 3-8**).

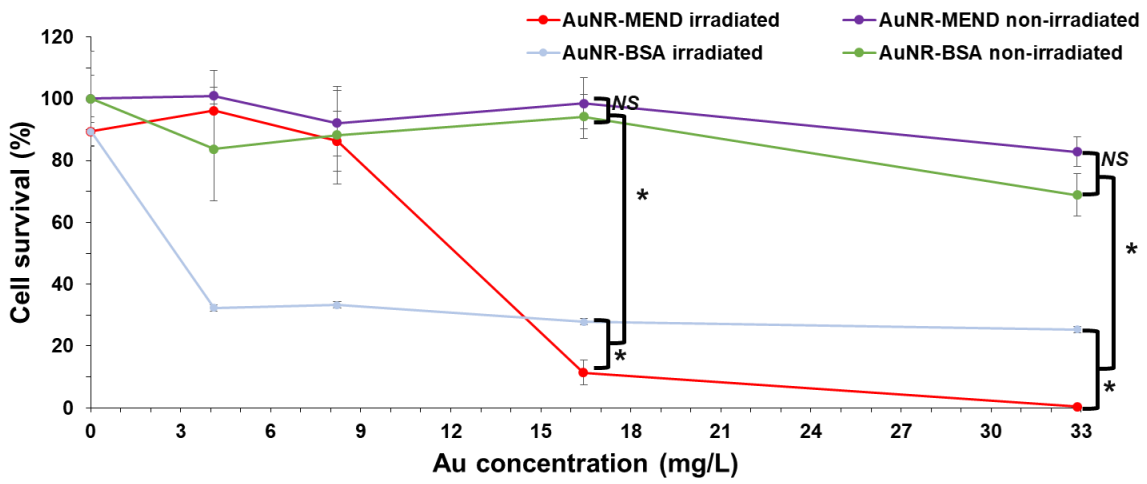

Figure 3-7. Dose-response curves for the cytotoxicity of AuNR-MEND, and AuNR-BSA, with and without NIR irradiation at 0.5 W/cm^2 for 6 min. Error bars represent ± S.D. for three different experiments performed in triplicate (**p<0.05, One-way ANOVA, Tukey's HSD).*

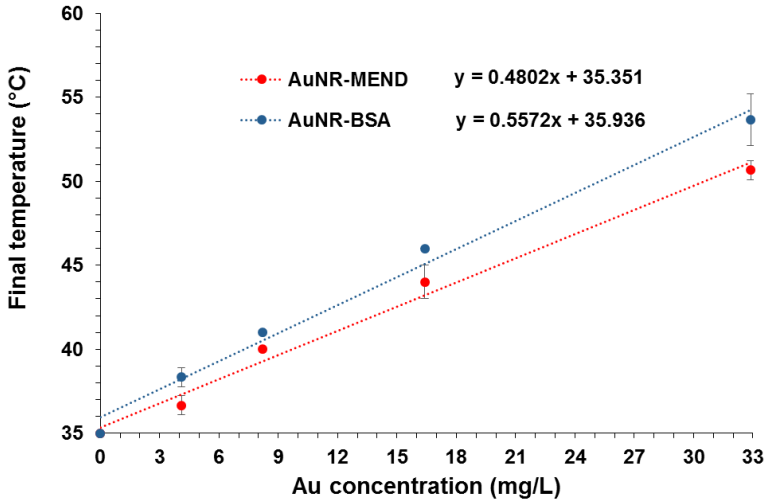

Figure 3-8. Dose-medium temperature curves for AuNR-MEND and AuNR-BSA after NIR irradiation for 6 min using 0.5 1.0 W light power. Error bars represent ± S.D. for three different experiments performed in triplicate.

4. Evaluation of cellular uptake

The cytotoxicity findings prompted the investigation of the homogeneity of cellular uptake for AuNR-MEND. AuNR-MEND was labeled with DiD, a fluorescent dye, and cellular uptake was then evaluated by fluorescence-assisted cell sorting (FACS) (**Figure 3-9**). In this DiD-labeling experiment, the AuNR-MEND was purified by centrifugation to remove empty liposomes that could cause false positive signals.

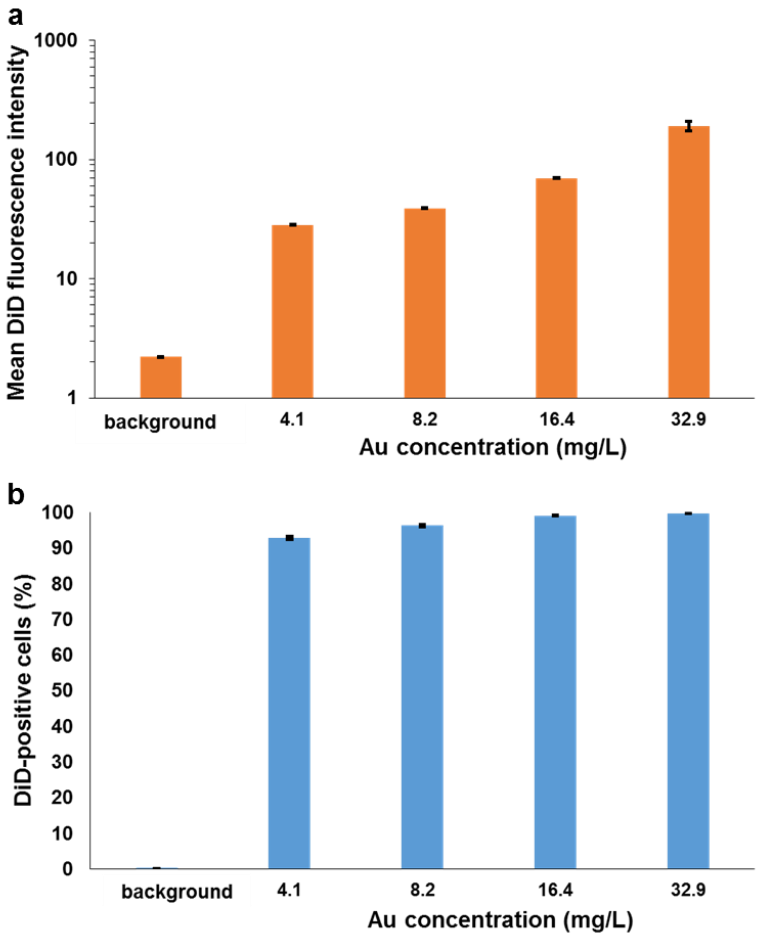

Figure 3-9. Cellular uptake measurement of AuNR-MEND in 4T1 cells. DiD-labeled AuNR-MENDs were incubated with 4T1 cells at the indicated concentrations, and then analyzed by FACS. Mean fluorescence intensities of DiD (a) and (b) percentage of DiD-positive cells (fluorescence intensity above 10) are shown. Error bars represent ± S.D. for three different experiments performed in triplicate.

Cellular uptake clearly increased with dose (**Figure 3-9-a**). Even at the lowest concentration, the AuNR-MEND was taken up by nearly 100% of the cell population (**Figure 3-9-b**). Therefore, the homogenous uptake of the AuNR-MEND by the cultured cells might be a key factor in the observed cell-killing activity (**Figure 3-7**). Cellular uptake was also confirmed based on CLSM images (**Figure 3-10**), which shows that the DiD signals from AuNR-MEND are clearly inside the cell borders and are near the nucleus. Targeting the nucleus has been reported to be beneficial for photothermal cytotoxicity[66]. Slight co-localization of AuNR-MEND with the endosomes was also observed (orange signals, **Figure 3-11**), which is expected with lipid nanoparticles containing ssPalmM[29]. However, cellular trafficking may be improved in the future with other ssPalm analogues.

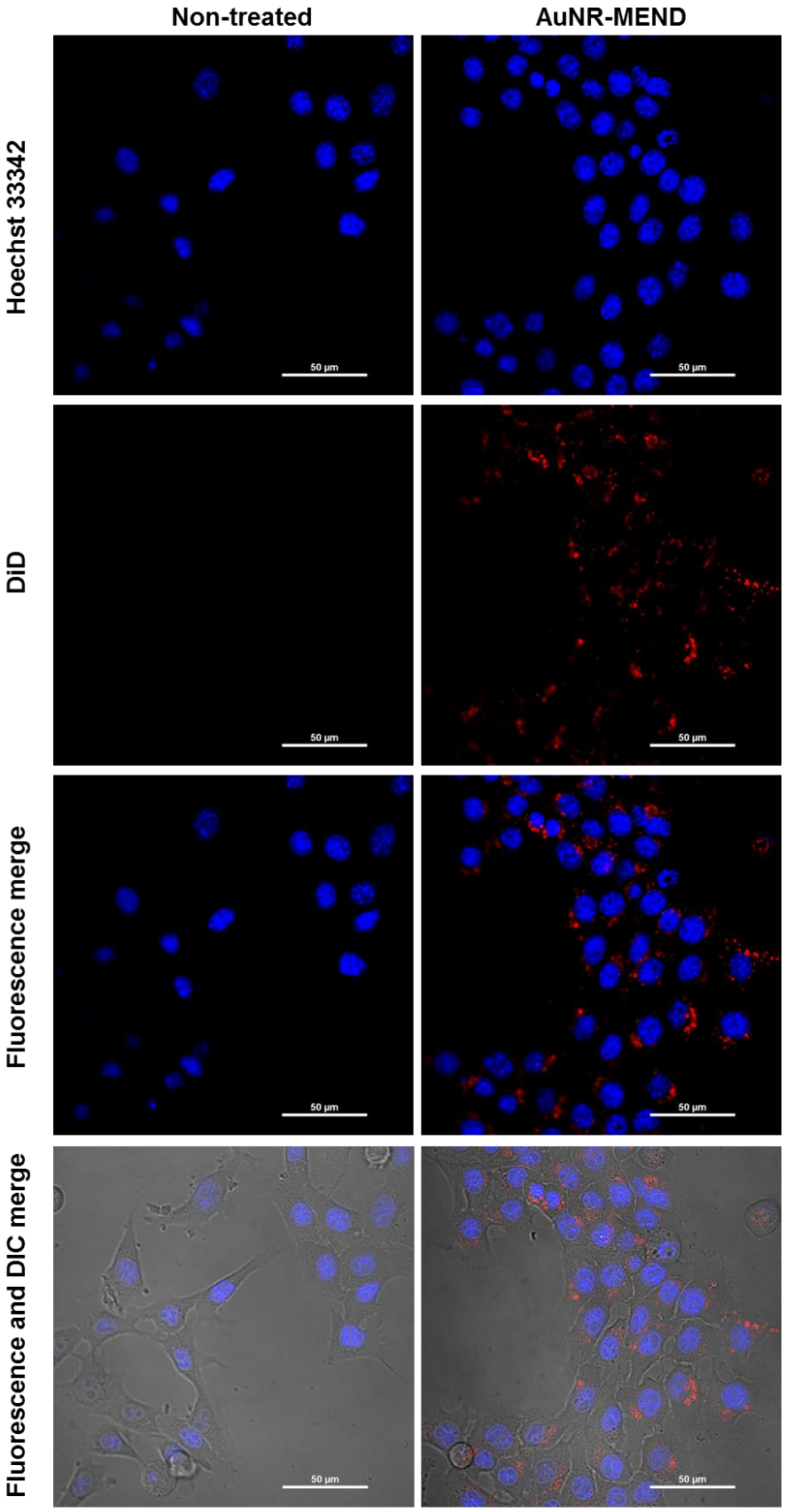

Figure 3-10. Evaluation of cellular uptake of AuNR-MEND using confocal microscopy. Cells on the right column were incubated with DiD-labeled AuNR-MEND (red). All cell nuclei were stained with Hoechst 33342 (blue). Merged images show the cell borders.

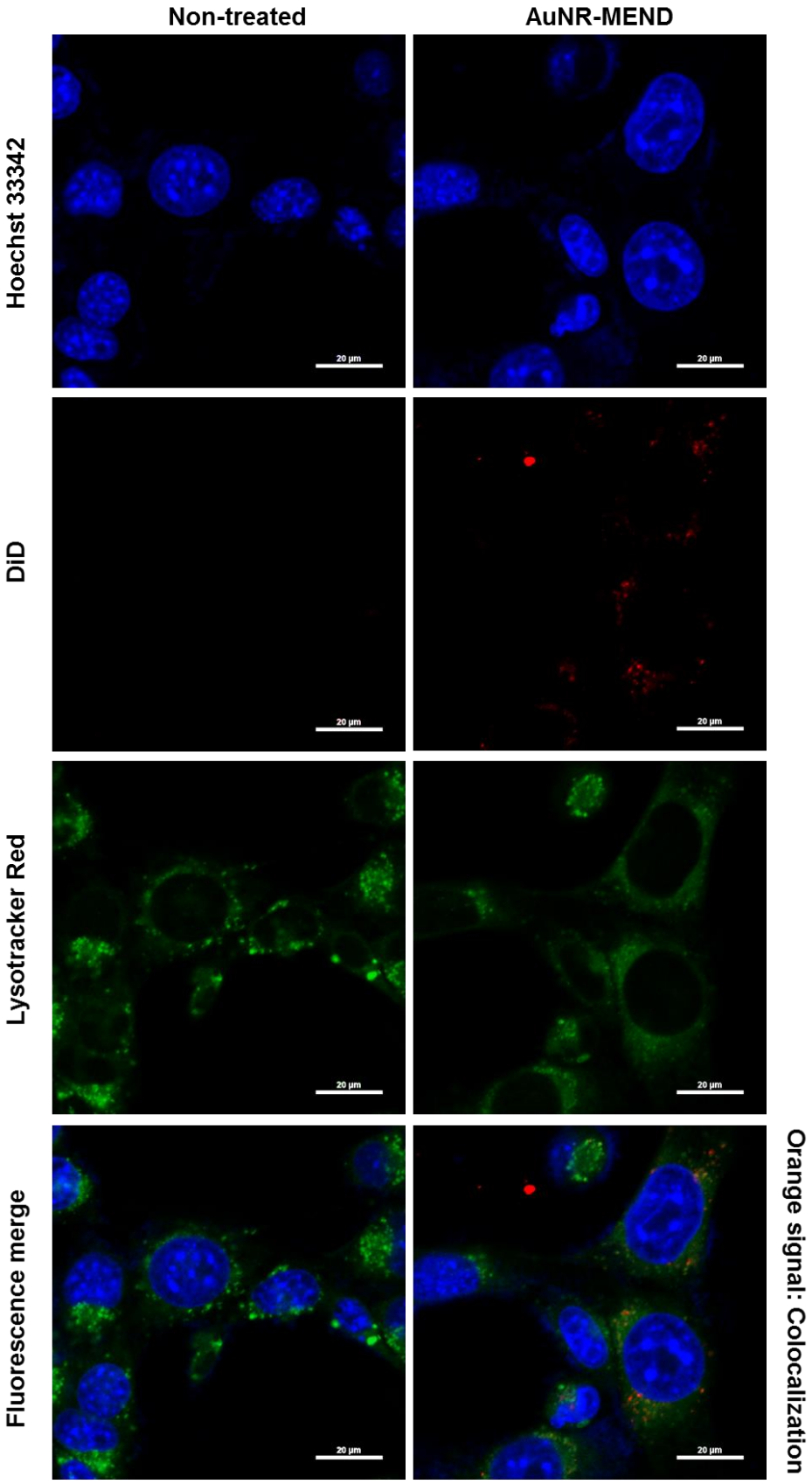

Figure 3-11. Evaluation of endosome co-localization. Cells were incubated with DiD-labeled AuNR-MEND (red). Cell nuclei and endosomes were stained with Hoechst 33342 (blue) and Lysotracker Red (green), respectively.

5. Measurement of caspase-3 production

Although direct thermal disruption of the membrane could also contribute to cell death[67], it has been previously reported that heat that is produced during photothermal therapy causes apoptosis through a caspase-dependent pathway[31,68]. Therefore caspase-3 activity as an index of the apoptosis induction[69] was explored.

After incubating the cells with AuNR-BSA or the AuNR-MEND (16.4 mg Au/L), followed by NIR irradiation at 0.5W/cm^2 for 6 min, the cells were further incubated with a specific caspase-3 substrate, N-Ac-DEVD-N'-MC-R110. The resulting cleavage product with a fluorescence at 535 nm was then measured[70]. The AuNR-MEND treatment caused a significant increase in caspase-3 activity in comparison with AuNR-BSA. (**Figure 3-12**), which may be attributed to the relatively low light power used in the assay[31]. Caspase-mediated apoptosis can be caused by AuNRs through mitochondrial damage[71]. Hence, damage to the mitochondria could have been possible as well.

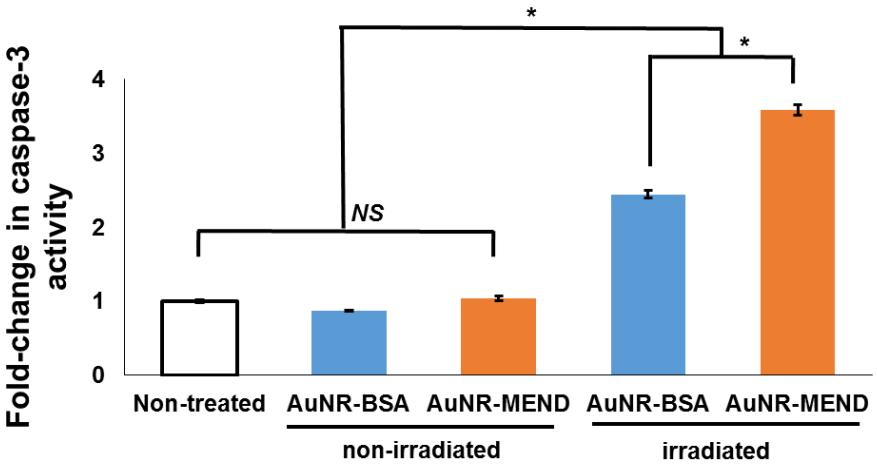

Figure 3-12. Measurement of caspase-3 activity after AuNR–BSA and AuNR-MEND treatment, with and without NIR irradiation. Activity was normalized to the percentage of surviving cells determined from WST-8 assay data. Error bars represent ± S.D. for five different experiments performed in triplicate. The mean fold-change in caspase-3 activity was not significantly different among the non-treated and non-irradiated cells. Among the irradiated groups, activity in AuNR-MEND-treated cells was significantly higher than in those treated with AuNR-BSA (**p<0.05, One-way ANOVA, Tukey's HSD*).

C. Conclusion

The photothermal cytotoxicity assay was designed and optimized to include irradiation of cells at 0.5 W/cm^2 for 6 min. AuNR-MEND demonstrated photothermal cytotoxicity which is stronger than that of previous formulations. The cell killing effect was caused by internalization of AuNR-MEND, and production of heat inside the cells. At a low dose, the NIR photothermal cytotoxicity of AuNR-BSA was higher than that for the AuNR-MEND. However, in higher doses, AuNR-MEND resulted in the complete destruction of the cells, while the cell survival rate reached a plateau at 30% in the case of AuNR-BSA. Its cellular uptake was also shown to be dose-dependent, supporting the dose-dependent cytotoxicity observed. Furthermore, apoptosis was also indicated to be the mechanism of cytotoxicity.

D. Experimental Section

1. Cell culture and in vitro photothermal cytotoxicity assay

Mouse mammary tumor (4T1) cells were obtained from the American Type Culture Collection (ATCC). They were maintained in RPMI-1640 medium (Sigma-Aldrich) supplemented with 10% fetal bovine serum (FBS), penicillin (100 U/mL) and streptomycin (100 µg/mL). The cell culture was maintained at 37 °C in a 5% CO_2, humidified incubator (**Figure S-3**)[72]. 4T1 cells were grown in 96-well tissue culture plates overnight. Thereafter, the growth media was removed and replaced with growth media containing AuNR at the indicated concentrations in terms of OD unit. The UV-Vis-NIR spectra of AuNR-MEND in growth media was not expected to be significantly altered when their environment was changed from water to growth media. After a 2 h incubation time, the cells were exposed to a Compact Xenon light source (Asahi Spectra MAX-303, 750-900 nm) at 0.5 to 1 W/cm^2 (spot size around 1 cm^2) for 3–6 minutes. During irradiation, the cell culture dishes were kept at 37 °C on a slide warmer (Tissue-Tek Slide Warmer PS-53, Sakura FineTek Japan). The temperature inside each well was measured by a thermocouple thermometer K-type (A&D AD-5602A, A&D Co., Ltd.). After 4 h, cell viability was determined using a CCK-8 kit (Dojindo Laboratories, Dojindo Molecular Technologies, Inc.) according to the manufacturer's protocol[64].

2. Confocal laser scanning microscopy (CLSM)

To examine the cellular uptake of the nanoparticles, the AuNR-MEND was labeled with DiD (Molecular Probes). For the labeling, DiD (0.5 mol% of total lipid) was included in the lipid composition during the preparation of the AuNR-MEND. 1 x 10^4 cells were seeded on a 3.5-cm glass base dish (Iwaki, Asahi Glass Co., Ltd.) in 2 mL of culture medium 1 day before the experiment. The growth media was removed and replaced with growth media containing the fluorescently-labeled nanoparticles at OD 0.5. The nanoparticles were incubated with the cells for 4 h. Cell surface-bound MENDs were removed by washing the cells twice with PBS. The nuclei were then stained with 5 μg/mL Hoechst 33342 (Dojindo Laboratories). The culture medium was changed to phenol red-free RPMI 1640 (Gibco) before microscopic observation. Confocal images were obtained using a Nikon A1 microscope equipped with a water immersion objective lens (Plan Apo 60x 1.20 PFS WI). Control of the microscopy and acquisition of digital images were performed with the NIS-Elements software (Nikon)[30]. For Hoechst 33342, a 405 nm laser was used for excitation and a 425–475 nm channel was used for detection, while for DiD, a 638 nm laser was used for excitation and a 662–737 nm channel was used for detection. The signals for Hoechst 33342 and DiD are blue and red, respectively.

Lysotracker Red DND-99 was used to stain endosomes (5 μL, 30 min before observation). A 561 nm laser was used for excitation and a 570–620 nm channel was used for detection (green signals).

3. Fluorescence-assisted cell sorting (FACS)

To examine the cellular uptake of the nanoparticles, AuNR-MEND were labeled with DiD (Molecular Probes). For the labeling, DiD (0.05 mol% of total lipid) was included in the lipid composition in the system used in the preparation of AuNR-MEND. The empty liposomes were removed by centrifugation at 1,000 g for 1 min. 4T1 cells ($1x10^5$ cells/well) were cultured on 6-well plates for 24 h prior to being used. The cells were then incubated with OD 0.125–1.0 of fluorescently-labeled AuNR-MEND. They were then washed 3 times with cold PBS and detached by

treatment with 0.05% trypsin, 0.55 mM ethylenediaminetetraacetic acid (EDTA) in PBS. The collected cells were then suspended in RPMI 1640 with FBS, and then centrifuged (100 rpm, 4°C, 5 min). The cells were washed with FACS buffer [0.5% BSA and 0.1% NaN_3 in PBS (−)], and then suspended again in FACS buffer. The suspended cells were filtered through a nylon mesh, and then fluorescence intensity was measured by FACS (FACSCalibur, Becton Dickinson, Franklin Labs, NJ) using FL-4 detector for DiD. Data were processed using Cell Quest (Becton Dickinson)[73].

4. Caspase-3 assay

4T1 cells were grown overnight in 96-well tissue culture plates. Thereafter, the growth media was removed and replaced with growth media containing AuNR-BSA or the AuNR-MEND (OD 0.5). After a 2 h incubation time, the cells were exposed to a Compact Xenon light source (Asahi Spectra MAX-303, 750-900 nm) at 0.5 to 1 W/cm^2 (spot size around 1 cm^2) for 6 min. During the irradiation, the cell culture dishes were kept at 37 °C on a slide warmer (Tissue-Tek Slide Warmer PS-53, Sakura FineTek Japan). After 4 h of additional incubation, the culture plate was centrifuged and caspase-3 activity was assayed using a caspase-3 fluorescence assay kit according to the manufacturer's protocol (Cayman Chemicals)[74]. Caspase-3 activity was normalized using the percentage of surviving cells taken from WST-8 assay data[75] using the following equation:

$$\text{fold-change in caspase-3 activity} = \frac{\text{activity}}{\text{percentage of surviving cells}}$$

The results were analyzed using one-way ANOVA performed at a 95% confidence level. Tukey's HSD was performed as post-hoc test.

Chapter IV: Assessment of Pharmacokinetics and Toxicity

A. Introduction

Solid tumors and inflamed tissues possess loose endothelial junctions, hence facilitating the enhanced permeability and retention (EPR) effect[76]. PEGylation of AuNRs have been reported to make use of this to passively target the tumor[39,55,77]. Majority of the injected nanoparticles still end up in the liver, which is the organ responsible for the fate of nanoparticles which are larger than 8 nm and could not be cleared by the kidneys through glomerular filtration[78]. This chapter explores the possibility of passive tumor targeting using AuNR-MEND by studying some pharmacokinetic parameters. The hepatotoxicity of AuNR-MEND was also explored.

B. Results and Discussion

1. Preparation of long-circulating AuNR-MEND

AuNR-MEND was prepared with 10 mol% of DSG-mPEG$_{2000}$ (instead of DMG-mPEG$_{2000}$) to increase its stability *in vivo*. PEGylation provides a “stealth effect” to the nanoparticle, lessening the chances that it will be captured by the RES. Long-circulating MEND labeled with DiD was injected intravenously into BALB/c mice (5w ♀). After 24 h, it can be seen that at least 20% of the original MEND concentration still remains (**Figure 4-1**). This means that the prepared MEND is long-circulating, through the stealth effect provided by PEG[79]. Around half is eliminated after approximately 8 h. Using literature data as comparison, AuNR-BSA has a very short half-life of 12 min[80,81]. On the other hand, only 5% of AuNR-CTAB remain in the blood after 30 min[82], making its half-life approximately similar to AuNR-BSA. However, longer circulating AuNRs covalently conjugated with PEG-5000 through a thiol moiety have been already previously prepared, with $t_{1/2}$ of 17 h[83].

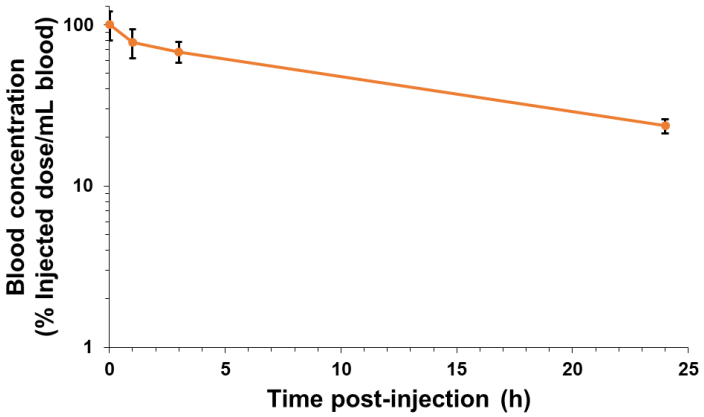

Figure 4-1. Blood clearance of AuNR-MEND. BALB/c mice were injected via the tail vein with DiD-labeled MEND. Data are expressed as the mean %ID/mL blood ± SD at 0.017, 1, 3 and 24 h after administration (n = 3).

2. Determination of tissue distribution

Because of the long circulation time, it is possible that the nanoparticles could have reached the tumor after 24 h through the EPR effect. Fluorescent labelling is a stable and biocompatible way to assess tissue distribution of liposomes[84], hence MEND was once again labeled with DiD. DiD-labeled MEND of the same dose were injected to 4T1 tumor-bearing mice (tumor volume = 57.5 ± 6.8 mm^3). The liver, spleen, kidney, and tumor tissues were collected, homogenized, and assayed for DiD concentration. Some tumor accumulation was observed, however, around 35% of the nanoparticle were captured by the mononuclear phagocyte system (MPS) and accumulated in the liver and spleen (**Figure 4-2**). This is expected since the relatively large particle size (151 nm) does not allow it to be eliminated by glomerular filtration (limit: 5.5 nm)[35]. This is supported by the low accumulation on the kidney. The liver and spleen are also highly vascularized filtration organs[85] and hence, after a long enough circulation period, the nanoparticles have indeed ended up in these organs.

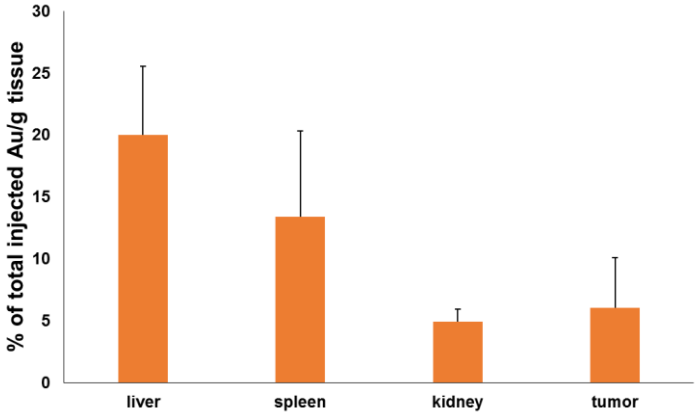

Figure 4-2. Tissue distribution profile of AuNR-MEND.

3. Assessment of liver toxicity

Since a large percentage accumulated on the liver, hepatotoxicity was checked by measuring liver function enzymes or serum transaminases (ALT and AST) after injection. The same dose was administered through the tail vein of BALB/c mice (5w♀). It was hypothesized that if AuNR-MEND damaged the liver, then the hepatocytes would release AST and ALT into extracellular space which would eventually be detected in the serum. Both AST and ALT were measured and their ratio was calculated. AST is released upon damage to liver and other tissues such as the smooth muscle while ALT release is specific only for the liver, so the ratio evaluates liver-specific damage[86].

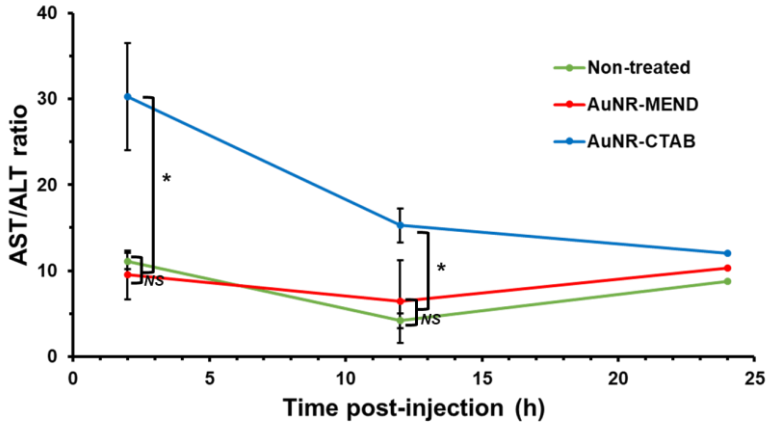

Figure 4-3. Toxicological analysis of AuNR-BSA- and AuNR-MEND-treated BALB/c mice. To assess the acute liver toxicity of MENDs, AST and ALT activities in serum were measured after a single intravenous administration at a dose of 40 μg/mouse *(n=3)*. The AST-ALT ratio was then calculated (**p<0.05, One-way ANOVA, Tukey's HSD*).

It was then observed that AuNR-MEND does not raise the AST/ALT ratio significantly, and has almost the same values as the non-treated mice. However, the AuNR-CTAB-treated group showed high AST/ALT ratio, from 2–12 h, indicating liver damage, with 1 mouse immediately dying after administration (**Figure 4-3**). This is expected, since AuNR-CTAB also accumulates in the liver and can cause non-specific cytotoxicity, as proven in previous studies[18]. CTAB concentration in the injected solution is estimated to be ~0.11 mM. AuNR-MEND is almost neutral, and this brings with it the advantage of not being hepatotoxic[46], as is expected of most drug delivery systems because of their non-toxic and biodegradable components[87].

C. Conclusion

AuNR-MEND modified with DSG-mPEG$_{2000}$ possessed long blood circulation properties and could accumulate in tumor after 24 h. it was also proven to be safe for *in vivo* applications because of its low hepatic toxicity, thereby eliminating CTAB-related non-specific toxicity.

D. Experimental Section

1. Animal handling experiments

BALB/c mice (♀, 5-week-old, 15-20 g in weight) were obtained from Japan SLC (Shizuoka, Japan). Tumor-bearing mice were prepared by anesthetization with diethyl ether, and subcutaneous inoculation of the right flanks with 1.0×10^6 4T1 cells. Animal handling procedures were reviewed and approved by the Hokkaido University Animal Care Committee in accordance with the Guide for the Care and Use of Laboratory Animals[72].

2. Measurement of AuNR-MEND in blood

DiD-labeled AuNR-MEND was administered intravenously to the tail vein at a dose of 40 μg Au/mouse. Blood samples were collected at 0.017, 1, 3, and 24 h after and rapidly mixed with 1% SDS. The fluorescent intensity of the mixture was measured with Infinite M200 (Tecan, Männedorf, Switzerland). Blood concentration was calculated by using a standard curve from the mixture of known amount of DiD-labeled AuNR-MEND and non-treated mice blood[88].

3. Tissue distribution analysis

DiD-labeled AuNR-MEND was administered intravenously to the tail vein at a dose of 40 μg Au/mouse. Mice were sacrificed after 24 h, and the liver, spleen, kidney, and tumor were collected. Each organ was weighed and minced. The tissues were then homogenized in 1% SDS and DiD fluorescence was measured from the homogenates using an Enspire microplate reader. The amount of nanoparticle found was calculated using a standard curve from a mixture of a known amount of tissue from a non-treated mouse and the injection solution.

4. Determination of liver enzymes

AuNR-MEND was administered intravenously to the tail vein at a dose of 40 μg Au/mouse. Blood samples were collected at 1, 6, and 24 h after administration. After collection, the blood samples were centrifuged at 800 g for 5 min at 4 °C. The supernatant was collected as serum samples, and then AST and ALT levels were measured using Wako Transaminase CII-Test kit (Wako Pure Chemical Industries Ltd. Osaka, Japan)[46].

Chapter V: Overall Conclusion and Future Perspectives

Au has been used in medicine for decades in the molecular form as aurothioglucose and gold sodium thiomalate for treatment of rheumatoid arthritis[89]. However, its applications in the nanoparticle form are novel and promising. The central goal of this research was to develop a method for encapsulating AuNRs in a non-toxic envelope, making it suitable for photothermal therapy. It was discovered that a protein was needed for this to be possible, with the encapsulation being proven through TEM. AuNR-MEND caused complete NIR-triggered cytotoxicity. This can be most probably attributed to homogenous cellular uptake. Apoptosis was determined as a possible mechanism of cytotoxicity. AuNR-MEND has also demonstrated long blood circulation time and tumor accumulation through the EPR effect, as well as the loss of hepatoxicity associated with CTAB. It has been demonstrated that coating AuNRs within a lipid envelope is a promising strategy for avoiding non-specific cytotoxicity derived from CTAB. It has also enhanced the photothermal effect and pharmacokinetics of the nanoparticles. Therefore, the main objective has been achieved.

The possibility of encapsulating AuNRs into MEND offers a wide range of future applications. Photothermal ablation of tumors can be achieved[6] by passive or active[68,90,91] targeting of tumor tissues even in the event of metastasis[92]. This has been proven many times in animal models but relying on this alone is not enough to attain selectivity, since AuNR-MEND is also responsible for particle accumulation in liver and spleen[76].

Improving the PTT effect can also be explored. The sensitivity of different cancer cells to hyperthermia is diverse and is regulated by several genes[93]. Those which have been treated with hyperthermia previously are prone to acquire resistance to heat stress. Hence, one strategy is to conjugate AuNRs with molecules that can combat heat resistance of tumors. Diclofenac, a glucose transporter (Glut1) inhibitor, has been reported to help overcome tolerance of cancer cells by interfering with anaerobic glycolysis, increasing the efficacy of AuNRs[9]. This can be attached to AuNR-MEND. Adding natural product molecules like quercetin can also be used to decrease production of heat-shock protein and to suppress tumor growth and

metastasis[94], consequently strengthening photothermal cytotoxicity through apoptosis[8].

Control or intracellular trafficking can be achieved using other derivatives of ssPalmM[29,30,95] or adding other surface molecules[96,37]. Targeting specific organelles like the nucleus[97] or the mitochondria[98] has also been reported to increase photothermal cytotoxicity. AuNR-MEND can also be used for combined photothermal and chemotherapy of known anti-cancer drugs[99–101] to increase the anticancer effect of either of these agents, since hyperthermia has been reported to improve drug delivery[102]. In connection with this, AuNRs can also be used as light-controlled release systems[103]. When coated with DNA, it can form core-satellite assemblies with Au nanospheres containing complementary DNA[104]. Hence, satellite assemblies with other nanoparticles are possible too. AuNR-MEND can also serve as platform for vaccine[62,105] and gene delivery[106,107] and can also be used for cancer cell imaging when conjugated to antibodies that can attach to specific cell surface markers[91,97].

Aside from theranostics, the surface-enhanced resonance properties of AuNR can also be harnessed for analytical applications such as biosensing[108,109]. Combining the potentials of liposomes and AuNRs may pave the way for vast prospects in nanomedicine.

To consolidate all researches on therapy using gold nanoparticles, a database containing data on all properties of the nanoparticle such as size, surface charge, type of surface ligand or coating material as well as information on the system it was tested on like cancer cell type, tumor model, biological effect, and tumor distribution may also be constructed[110–112]. This will greatly enable researchers to perform their own analyses and pick out the properties that can produce the most optimum biological effect.

Supplementary Information

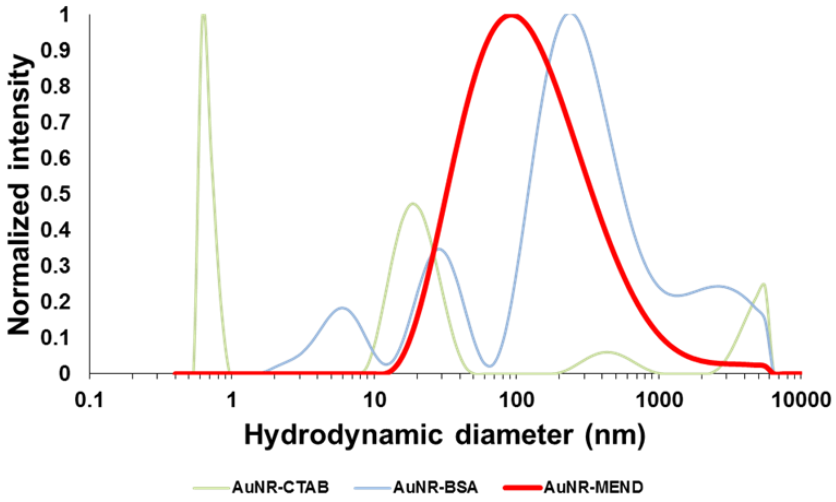

Figure S-1. Size distribution profiles of AuNR-CTAB, AuNR-BSA, and AuNR-MEND as evaluated by DLS.

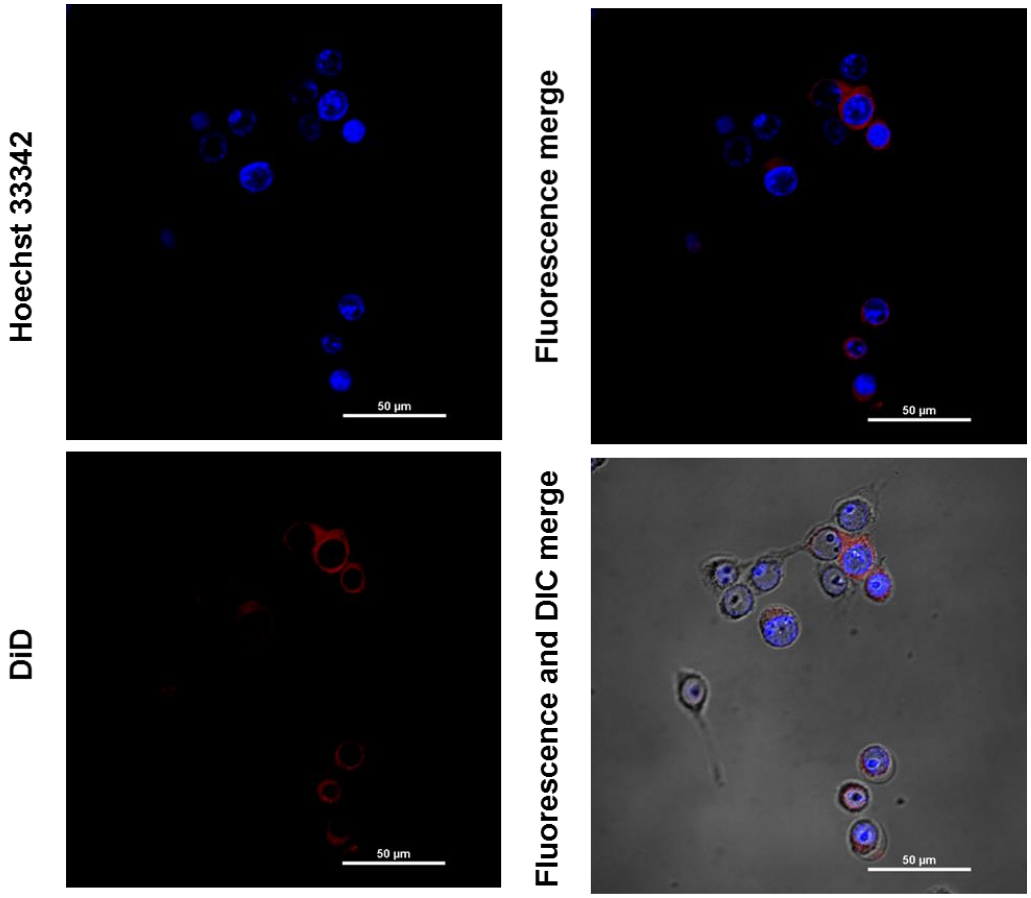

Figure S-2. CLSM images of cells were incubated with DiD-labeled AuNR-CTAB (red), showing its cytotoxic effect. Cell nuclei were stained with Hoechst 33342 (blue).

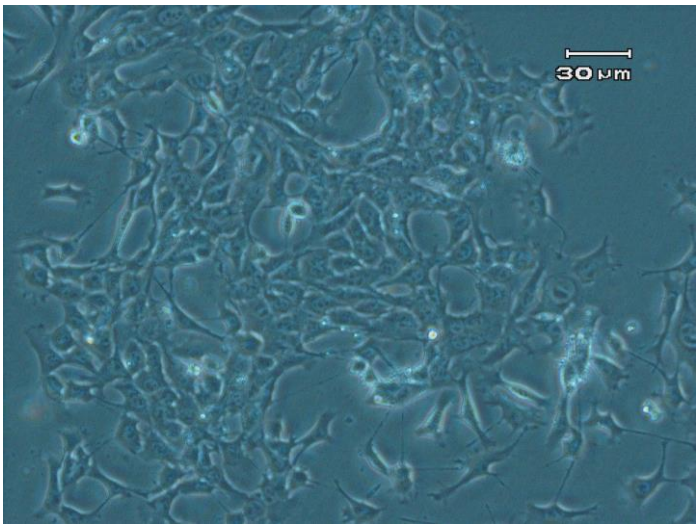

Figure S-3. 4T1 mouse mammary tumor cells under light microscope.

Abbreviations

AuNR – gold nanorod

ALT – alanine aminotransferase

AST – aspartate aminotransferase

BSA – bovine serum albumin

CCK-8 – cell counting kit

CLSM – confocal scanning laser microscopy

CTAB – cetyltrimethylammonium bromide

DMG-mPEG$_{2000}$ – 1,2-dimyristoyl-sn-glycerol, methoxypolyethylene glycol

DSG-mPEG$_{2000}$ – 1,2-distearoyl-sn-glycerol, methoxypolyethylene glycol

DOPE - 1,2-dioleoyl-sn-glycero-3-phosphoethanolamine

EDTA – ethylenediaminetetraacetic acid

EPR – enhanced permeability and retention

FACS – fluorescence-assisted cell sorting

FBS – fetal bovine serum

Hb – hemoglobin

HbO_2 – oxyhemoglobin

Glut1 – glucose transporter 1

ICP-AES – inductively-coupled plasma atomic emission spectroscopy

LSPR – longitudinal surface plasmon resonance

MCA – mercaptocarboxylic acid

MEND – multifunctional envelope-type nano device

MPS – mononuclear phagocyte system

NIR – near infra-red

OD – optical density

PBS – phosphate-buffered saline

pDNA – plasmid deoxyribonucleic acid

PLL – polylysine

POPC – 1-palmitoyl-2-oleoyl-sn-glycero-3-phosphocholine

PSS – polystyrenesulfonate

PTT – photothermal therapy

PVP – polyvinylpyrrolidone

RES – reticuloendothelial system

RPMI – Roswell Park Memorial Institute

SERS – surface-enhanced Raman spectroscopy

siRNA – small interference ribonucleic acid

ssPalm – S-S cleavable proton-activated lipid-like material

TEM – transmission electron microscopy

TNFα – tumor necrosis factor alpha

WST-8 – water-soluble tetrazolium

References

[1] E.C. Dreaden, A.M. Alkilany, X. Huang, C.J. Murphy, M.A. El-Sayed, The Golden Age: Gold Nanoparticles for Biomedicine, Chem. Soc. Rev. 41 (2012) 2740–2779. doi:10.1039/c1cs15237h.

[2] Gold Nanoparticles: Properties and Applications | Sigma-Aldrich, (n.d.). http://www.sigmaaldrich.com/technical-documents/articles/materials-science/nanomaterials/gold-nanoparticles.html (accessed June 19, 2017).

[3] N. Grimaldi, F. Andrade, N. Segovia, L. Ferrer-Tasies, S. Sala, J. Veciana, N. Ventosa, Lipid-based nanoversicles for nanomedicine, 45 (2016) 6520–6545. http://www.ncbi.nlm.nih.gov/pubmed/27722570 (accessed June 17, 2017).

[4] S.K. Libutti, G.F. Paciotti, A.A. Byrnes, H.R. Alexander, W.E. Gannon, M. Walker, G.D. Seidel, N. Yuldasheva, L. Tamarkin, Phase I and pharmacokinetic studies of CYT-6091, a novel PEGylated colloidal gold-rhTNF nanomedicine, Clin. Cancer Res. 16 (2010) 6139–6149. doi:10.1158/1078-0432.CCR-10-0978.

[5] 2014 Physics Problems | IPT, (n.d.). http://ipt.epfl.ch/problems (accessed June 19, 2017).

[6] M.A. El-Sayed, A.A. Shabaka, O.A. El-Shabrawy, N.A. Yassin, S.S. Mahmoud, S.M. El-Shenawy, E. Al-Ashqar, W.H. Eisa, N.M. Farag, M.A. El-Shaer, N. Salah, A.M. Al-Abd, Tissue Distribution and Efficacy of Gold Nanorods Coupled with Laser Induced Photoplasmonic Therapy in Ehrlich Carcinoma Solid Tumor Model, PLoS One. 8 (2013) 1–9. doi:10.1371/journal.pone.0076207.

[7] S.E. Lohse, C.J. Murphy, The Quest for Shape Control: A History of Gold Nanorod Synthesis, Chem. Mater. 25 (2013) 1250–1261. doi:10.1021/cm303708p.

[8] M.R.K. Ali, H.R. Ali, C.R. Rankin, M.A. El-Sayed, Targeting heat shock protein 70 using gold nanorods enhances cancer cell apoptosis in low dose plasmonic photothermal therapy, Biomaterials. 102 (2016) 1–8. doi:10.1016/j.biomaterials.2016.06.017.

[9] W.-H. Chen, G.-F. Luo, Q. Lei, S. Hong, W.-X. Qiu, L.-H. Liu, S.-X. Cheng, X.-Z. Zhang, Overcoming the Heat Endurance of Tumor Cells by Interfering with

the Anaerobic Glycolysis Metabolism for Improved Photothermal Therapy., ACS Nano. 11 (2017) 1419–1431. doi:10.1021/acsnano.6b06658.

[10] K. Engin, D.B. Leeper, L. Tupchong, F.M. Waterman, Thermoradiotherapy in the management of superficial malignant tumors., Clin. Cancer Res. 1 (1995).

[11] K. Engin, Biological rationale and clinical experience with hyperthermia., Control. Clin. Trials. 17 (1996) 316–42. http://www.ncbi.nlm.nih.gov/pubmed/8889346 (accessed December 16, 2016).

[12] E.C. Dreaden, L.A. Austin, M.A. Mackey, M.A. El-Sayed, Size matters: gold nanoparticles in targeted cancer drug delivery, Ther. Deliv. 3 (2012) 457–478. doi:10.4155/tde.12.21.

[13] M.F. Tsai, S.H.G. Chang, F.Y. Cheng, V. Shanmugam, Y.S. Cheng, C.H. Su, C.S. Yeh, Au nanorod design as light-absorber in the first and second biological near-infrared windows for in vivo photothermal therapy, ACS Nano. 7 (2013) 5330–5342. doi:10.1021/nn401187c.

[14] M.R.K. Ali, B. Snyder, M.A. El-Sayed, Synthesis and Optical Properties of Small Au Nanorods Using a Seedless Growth Technique, Langmuir. 28 (2012) 9807–9815. doi:10.1021/la301387p.

[15] R. Weissleder, A clearer vision for in vivo imaging Progress continues in the development of smaller , more penetrable probes for biological imaging . Toward the phosphoproteome, Nat. Biotechnol. 19 (2001) 316–317. doi:10.1038/86684.

[16] J. Wan, J.-H. Wang, T. Liu, Z. Xie, X. Yu, W. Li, Surface chemistry but not aspect ratio mediates the biological toxicity of gold nanorods in vitro and in vivo, Sci. Rep. 5 (2015) 11398. doi:10.1038/srep11398.

[17] L. Wang, X. Jiang, Y. Ji, R. Bai, Y. Zhao, X. Wu, C. Chen, Surface chemistry of gold nanorods: origin of cell membrane damage and cytotoxicity, Nanoscale. 5 (2013) 8384. doi:10.1039/c3nr01626a.

[18] E. Yasun, C. Li, I. Barut, D. Janvier, L. Qiu, C. Cui, W. Tan, BSA modification to reduce CTAB induced nonspecificity and cytotoxicity of aptamer-conjugated gold nanorods, Nanoscale. 7 (2015) 10240–10248. doi:10.1039/c5nr01704a.

[19] T.M. Allen, P.R. Cullis, Liposomal drug delivery systems: From concept to clinical applications, Adv. Drug Deliv. Rev. 65 (2013) 36–48. http://www.sciencedirect.com/science/article/pii/S0169409X12002980.

[20] M. Lanzrein, A. Schlegel, C. Kempf, Entry and uncoating of enveloped viruses,

Biochem. J. 302 (1994) 313–320. doi:10.1042/bj3020313.

[21] K. Kogure, H. Akita, Y. Yamada, H. Harashima, Multifunctional envelope-type nano device (MEND) as a non-viral gene delivery system, Adv. Drug Deliv. Rev. 60 (2008) 559–571. doi:10.1016/j.addr.2007.10.007.

[22] M. Hyodo, Y. Sakurai, H. Akita, H. Harashima, “Programmed packaging” for gene delivery, J. Control. Release. 193 (2014) 316–323. doi:10.1016/j.jconrel.2014.04.023.

[23] H. Hatakeyama, H. Akita, H. Harashima, A multifunctional envelope type nano device (MEND) for gene delivery to tumours based on the EPR effect: A strategy for overcoming the PEG dilemma, Adv. Drug Deliv. Rev. 63 (2011) 152–160. doi:10.1016/j.addr.2010.09.001.

[24] Molecular Expressions Cell Biology: The Influenza (Flu) Virus, (n.d.). https://micro.magnet.fsu.edu/cells/viruses/influenzavirus.html (accessed June 19, 2017).

[25] Y. Sato, T. Nakamura, Y. Yamada, H. Harashima, Development of a multifunctional envelope-type nano device and its application to nanomedicine, J. Control. Release. 244 (2016) 194–204. doi:10.1016/j.jconrel.2016.06.042.

[26] Y. Sato, Y. Sakurai, K. Kajimoto, T. Nakamura, Y. Yamada, H. Akita, H. Harashima, Innovative Technologies in Nanomedicines: from Passive Targeting to Active Targeting/from Controlled Pharmacokinetics to Controlled Intracellular Pharmacokinetics, Macromol. Biosci. (2016). doi:10.1002/mabi.201600179.

[27] S.C. Semple, A. Akinc, J. Chen, A.P. Sandhu, B.L. Mui, C.K. Cho, D.W.Y. Sah, D. Stebbing, E.J. Crosley, E. Yaworski, I.M. Hafez, J.R. Dorkin, J. Qin, K. Lam, K.G. Rajeev, K.F. Wong, L.B. Jeffs, L. Nechev, M.L. Eisenhardt, M. Jayaraman, M. Kazem, M.A. Maier, M. Srinivasulu, M.J. Weinstein, Q. Chen, R. Alvarez, S.A. Barros, S. De, S.K. Klimuk, T. Borland, V. Kosovrasti, W.L. Cantley, Y.K. Tam, M. Manoharan, M.A. Ciufolini, M.A. Tracy, A. de Fougerolles, I. MacLachlan, P.R. Cullis, T.D. Madden, M.J. Hope, Rational design of cationic lipids for siRNA delivery, Nat. Biotechnol. 28 (2010) 172–176. doi:10.1038/nbt.1602.

[28] A.K. Varkouhi, M. Scholte, G. Storm, H.J. Haisma, Endosomal escape pathways for delivery of biologicals, J. Control. Release. 151 (2011) 220–228. doi:10.1016/j.jconrel.2010.11.004.

[29] H. Akita, R. Ishiba, H. Hatakeyama, H. Tanaka, Y. Sato, K. Tange, M. Arai, K. Kubo, H. Harashima, A neutral envelope-type Nanoparticle containing pH-responsive and SS-Cleavable lipid-like material as a carrier for Plasmid DNA, Adv. Healthc. Mater. 2 (2013) 1120–1125. doi:10.1002/adhm.201200431.

[30] H. Tanaka, H. Akita, R. Ishiba, K. Tange, M. Arai, K. Kubo, H. Harashima, Neutral biodegradable lipid-envelope-type nanoparticle using vitamin a-scaffold for nuclear targeting of plasmid DNA, Biomaterials. 35 (2014) 1755–1761. doi:10.1016/j.biomaterials.2013.11.016.

[31] J.R. Melamed, R.S. Edelstein, E.S. Day, Elucidating the fundamental mechanisms of cell death triggered by photothermal therapy, ACS Nano. 9 (2015) 6–11. doi:10.1021/acsnano.5b00021.

[32] M.R.K. Ali, Y. Wu, T. Han, X. Zang, H. Xiao, Y. Tang, R. Wu, F.M. Fernández, M.A. El-Sayed, Simultaneous Time-Dependent Surface-Enhanced Raman Spectroscopy, Metabolomics, and Proteomics Reveal Cancer Cell Death Mechanisms Associated with Gold Nanorod Photothermal Therapy, J. Am. Chem. Soc. 138 (2016) 15434–15442. doi:10.1021/jacs.6b08787.

[33] J.G. Mehtala, D.Y. Zemlyanov, J.P. Max, N. Kadasala, S. Zhao, A. Wei, Citrate-Stabilized Gold Nanorods, Lang. 30 (2014) 13727–13730. doi:10.1021/la5029542.

[34] A.P. Leonov, J. Zheng, J.D. Clogston, S.T. Stern, A.K. Patri, A. Wei, Detoxification of gold nanorods by treatment with polystyrenesulfonate, ACS Nano. 2 (2008) 2481–2488. doi:10.1021/nn800466c.

[35] E.C. Dreaden, M.A. Mackey, X. Huang, B. Kang, M.A. El-Sayed, Beating cancer in multiple ways using nanogold, Chem. Soc. Rev. 40 (2011) 3391. doi:10.1039/c0cs00180e.

[36] J. Alper, K. Hamad-Schifferli, Effect of ligands on thermal dissipation from gold nanorods, Langmuir. 26 (2010) 3786–3789. doi:10.1021/la904855s.

[37] I. Garcia, A. Sanchez-Iglesias, M. Henriksen-Lacey, M. Grzelczak, S. Penades, L.M. Liz-Marzan, Glycans as Biofunctional Ligands for Gold Nanorods: Stability and Targeting in Protein-Rich Media, J. Am. Chem. Soc. 137 (2015) 3686–3692. doi:10.1021/jacs.5b01001.

[38] C. Grabinski, N. Schaeublin, A. Wijaya, H. D'Couto, S.H. Baxamusa, K. Hamad-Schifferli, S.M. Hussain, Effect of gold nanorod surface chemistry on cellular response., ACS Nano. 5 (2011) 2870–2879. doi:10.1021/nn103476x.

[39] Z. Zhang, M. Lin, Fast loading of PEG–SH on CTAB-protected gold nanorods, RSC Adv. 4 (2014) 17760. doi:10.1039/c3ra48061e.

[40] C.J. Orendorff, T.M. Alam, D.Y. Sasaki, B.C. Bunker, J.A. Voigt, Phospholipid-gold nanorod composites, ACS Nano. 3 (2009) 971–983. doi:10.1021/nn900037k.

[41] L. Scarabelli, A. Sánchez-Iglesias, J. Pérez-Juste, L.M. Liz-Marzán, A “Tips and Tricks” Practical Guide to the Synthesis of Gold Nanorods, J. Phys. Chem. Lett. 6 (2015) 4270–4279. doi:10.1021/acs.jpclett.5b02123.

[42] G. Gramlich, J. Zhang, W.M. Nau, Increased antioxidant reactivity of vitamin C at low pH in model membranes., J. Am. Chem. Soc. 124 (2002) 11252–3. http://www.ncbi.nlm.nih.gov/pubmed/12236723 (accessed June 12, 2017).

[43] S. Park, N. Sinha, K. Hamad-Schifferli, Effective Size and Zeta Potential of Nanorods by Ferguson Analysis, Langmuir. 26 (2010) 13071–13075. doi:10.1021/la1024108.

[44] M.A. Mackey, M.R.K. Ali, L.A. Austin, R.D. Near, M.A. El-Sayed, The Most Effective Gold Nanorod Size for Plasmonic Photothermal Therapy : Theory and In Vitro Experiments The Most Effective Gold Nanorod Size for Plasmonic Photothermal Therapy : Theory and In Vitro Experiments, J. Phys. Chem. B. 118 (2014) 1319–1326. doi:10.1021/jp409298f.

[45] T. Murakami, H. Nakatsuji, N. Morone, J.E. Heuser, F. Ishidate, M. Hashida, H. Imahori, Mesoscopic metal nanoparticles doubly functionalized with natural and engineered lipidic dispersants for therapeutics, ACS Nano. 8 (2014) 7370–7376. doi:10.1021/nn5024818.

[46] M. Ukawa, H. Akita, Y. Hayashi, R. Ishiba, K. Tange, M. Arai, K. Kubo, Y. Higuchi, K. Shimizu, S. Konishi, M. Hashida, H. Harashima, Neutralized nanoparticle composed of SS-cleavable and pH-activated lipid-like material as a long-lasting and liver-specific gene delivery system, Adv. Healthc. Mater. 3 (2014) 1222–1229. doi:10.1002/adhm.201300629.

[47] N. Lozano, W.T. Al-Jamal, A. Taruttis, N. Beziere, N.C. Burton, J. Van den Bossche, M. Mazza, E. Herzog, V. Ntziachristos, K. Kostarelos, Liposome-gold nanorod hybrids for high-resolution visualization deep in tissues, J. Am. Chem. Soc. 134 (2012) 13256–13258. doi:10.1021/ja304499q.

[48] A. Taruttis, N. Lozano, A. Nunes, D.A. Jasim, N. Beziere, E. Herzog, K. Kostarelos, V. Ntziachristos, siRNA liposome-gold nanorod vectors for

multispectral optoacoustic tomography theranostics, Nanoscale. 6 (2014) 13451–13456. doi:10.1039/C4NR04164J.

[49] E. Ablinger, S. Wegscheider, W. Keller, R. Prassl, A. Zimmer, Effect of protamine on the solubility and deamidation of human growth hormone, Int. J. Pharm. 427 (2012) 209–216. doi:10.1016/j.ijpharm.2012.01.061.

[50] R. Balhorn, The protamine family of sperm nuclear proteins., Genome Biol. 8 (2007) 227. doi:10.1186/gb-2007-8-9-227.

[51] R.K. DeLong, L. Cillessen, C. Reynolds, A. Wanekaya, T. Severs, K. Ghosh, M. Fisher, S. Barber, J. Black, A. Schaeffer, K.J. Flores, Biomolecular Triconjugates Formed between Gold, Protamine, and Nucleic Acid: Comparative Characterization on the Nanoscale, J. Nanotechnol. 2012 (2012) 1–9. doi:10.1155/2012/954601.

[52] M. Tebbe, C. Kuttner, M. Männel, A. Fery, M. Chanana, Colloidally stable and surfactant-free protein-coated gold nanorods in biological media, ACS Appl. Mater. Interfaces. 7 (2015) 5984–5991. doi:10.1021/acsami.5b00335.

[53] N. Thioune, N. Lidgi-Guigui, M. Cottat, A.-M. Gabudean, M. Focsan, H.-M. Benoist, S. Astilean, M.L. de la Chapelle, Study of gold nanorods–protein interaction by localized surface plasmon resonance spectroscopy, Gold Bull. 46 (2013) 275–281. doi:10.1007/s13404-013-0118-5.

[54] S. Alam, A. Mukhopadhyay, Conjugation of gold Nanorods with bovine serum albumin protein, J. Phys. Chem. C. 118 (2014) 27459–27464. doi:10.1021/jp5093465.

[55] F. Scaletti, A. Feis, S. Centi, R. Pini, V.M. Rotello, L. Messori, Tuning the interactions of PEG-coated gold nanorods with BSA and model proteins through insertion of amino or carboxylate groups., J. Inorg. Biochem. 150 (2015) 120–5. doi:10.1016/j.jinorgbio.2015.04.016.

[56] A. Bujacz, Structures of bovine, equine and leporine serum albumin, Acta Crystallogr. Sect. D Biol. Crystallogr. 68 (2012) 1278–1289. doi:10.1107/S0907444912027047.

[57] H. Jiang, D. Chen, D. Guo, N. Wang, Y. Su, X. Jin, G. Tong, X. Zhu, Zwitterionic gold nanorods: low toxicity and high photothermal efficacy for cancer therapy, Biomater. Sci. 5 (2017) 686–697. doi:10.1039/C6BM00918B.

[58] X. Xu, A. Costa, D.J. Burgess, Protein encapsulation in unilamellar liposomes: High encapsulation efficiency and a novel technique to assess lipid-protein

interaction, Pharm. Res. 29 (2012) 1919–1931. doi:10.1007/s11095-012-0720-x.

[59] C. Payerl, M. Bračič, A. Zankel, W.J. Fischer, M. Kaschowitz, E. Fröhlich, R. Kargl, F. Stelzer, S. Spirk, Nonspecific protein adsorption on cationically modified Lyocell fibers monitored by zeta potential measurements, Carbohydr. Polym. 164 (2017) 49–56. doi:10.1016/j.carbpol.2017.01.088.

[60] H. Liu, N. Pierre-Pierre, Q. Huo, Dynamic light scattering for gold nanorod size characterization and study of nanorod-protein interactions, Gold Bull. 45 (2012) 187–195. doi:10.1007/s13404-012-0067-4.

[61] K. Niikura, K. Kobayashi, C. Takeuchi, N. Fujitani, S. Takahara, T. Ninomiya, K. Hagiwara, H. Mitomo, Y. Ito, Y. Osada, K. Ijiro, Amphiphilic gold nanoparticles displaying flexible bifurcated ligands as a carrier for siRNA delivery into the cell cytosol, ACS Appl. Mater. Interfaces. 6 (2014) 22146–22154. doi:10.1021/am505577j.

[62] K. Niikura, T. Matsunaga, T. Suzuki, S. Kobayashi, H. Yamaguchi, Y. Orba, A. Kawaguchi, H. Hasegawa, K. Kajino, T. Ninomiya, K. Ijiro, H. Sawa, Gold Nanoparticles as a Vaccine Platform: Influence of Size and Shape on Immunological Responses *in Vitro* and *in Vivo*, ACS Nano. 7 (2013) 3926–3938. doi:10.1021/nn3057005.

[63] R.C. Taylor, S.P. Cullen, S.J. Martin, Apoptosis: controlled demolition at the cellular level, Nat. Rev. Mol. Cell Biol. 9 (2008) 231–241. doi:10.1038/nrm2312.

[64] Dojindo, Cell Counting Kit-8 Technical Manual, 8 (2009) 1–7. www.dojindo.com.

[65] J.C.Y. Kah, C. Grabinski, E. Untener, C. Garrett, J. Chen, D. Zhu, S.M. Hussain, K. Hamad-Schifferli, Protein Coronas on gold Nanorods Passivated with Amphiphilic ligands affect Cytotoxicity and cellular response to penicillin/Streptomycin, ACS Nano. 8 (2014) 4608–4620. doi:10.1021/nn5002886.

[66] L. Pan, J. Liu, J. Shi, Nuclear-Targeting Gold Nanorods for Extremely Low NIR Activated Photothermal Therapy, ACS Appl. Mater. Interfaces. 9 (2017) 15952–15961. doi:10.1021/acsami.7b03017.

[67] L. Tong, Y. Zhao, T.B. Huff, M.N. Hansen, A. Wei, J.-X. Cheng, Gold Nanorods mediate tumor cell death by compromising membrane integrity, Adv. Mater. 19 (2007) 3136–3141. doi:10.1002/adma.200701974.

[68] S. Zhang, Y. Li, X. He, S. Dong, Y. Huang, X. Li, Y. Li, C. Jin, Y. Zhang, Y. Wang, Photothermolysis mediated by gold nanorods modified with EGFR monoclonal antibody induces Hep-2 cells apoptosis in vitro and in vivo., Int. J. Nanomedicine. 9 (2014) 1931–46. doi:10.2147/IJN.S59870.

[69] V. De Matteis, M.A. Malvindi, A. Galeone, V. Brunetti, E. De Luca, S. Kote, P. Kshirsagar, S. Sabella, G. Bardi, P.P. Pompa, Negligible particle-specific toxicity mechanism of silver nanoparticles: The role of Ag+ ion release in the cytosol, Nanomedicine Nanotechnology, Biol. Med. 11 (2015) 731–739. doi:10.1016/j.nano.2014.11.002.

[70] Z.-Q. Wang, J. Liao, Z. Diwu, N-DEVD-N'-morpholinecarbonyl-rhodamine 110: novel caspase-3 fluorogenic substrates for cell-based apoptosis assay., Bioorg. Med. Chem. Lett. 15 (2005) 2335–8. doi:10.1016/j.bmcl.2005.02.081.

[71] F. Zhang, X. Zhu, J. Gong, Y. Sun, D. Chen, J. Wang, Y. Wang, M. Guo, W. Li, Lysosome-mitochondria-mediated apoptosis specifically evoked in cancer cells induced by gold nanorods., Nanomedicine (Lond). 11 (2016) 1993–2006. doi:10.2217/nnm-2016-0139.

[72] T. Hada, Y. Sakurai, H. Harashima, Optimization of a siRNA Carrier Modified with a pH-Sensitive Cationic Lipid and a Cyclic RGD Peptide for Efficiently Targeting Tumor Endothelial Cells., Pharmaceutics. 7 (2015) 320–33. doi:10.3390/pharmaceutics7030320.

[73] Y. Yamada, M. Hashida, Y. Hayashi, M. Tabata, M. Hyodo, M.N. Ara, N. Ohga, K. Hida, H. Harashima, An approach to transgene expression in liver endothelial cells using a liposome-based gene vector coated with hyaluronic acid, J. Pharm. Sci. 102 (2013) 3119–3127. doi:10.1002/jps.23480.

[74] Cayman, Caspase-3 Fluorescence Assay Kit, (n.d.).

[75] A. Forbes, S. Anoopkumar-Dukie, R. Chess-Williams, C. McDermott, Relative cytotoxic potencies and cell death mechanisms of α_1 -adrenoceptor antagonists in prostate cancer cell lines, Prostate. 76 (2016) 757–766. doi:10.1002/pros.23167.

[76] R. Korsmeyer, Critical questions in development of targeted nanoparticle therapeutics, Regen. Biomater. 3 (2016) 143–147. doi:10.1093/rb/rbw011.

[77] T. Gong, D. Goh, M. Olivo, K.T. Yong, In vitro toxicity and bioimaging studies of gold nanorods formulations coated with biofunctional thiol-PEG molecules and pluronic block copolymers, Beilstein J. Nanotechnol. 5 (2014) 546–553.

doi:10.3762/bjnano.5.64.

[78] M. Bartneck, T. Ritz, H.A. Keul, M. Wambach, J. Bornemann, U. Gbureck, J. Ehling, T. Lammers, F. Heymann, N. Gassler, T. Lüdde, C. Trautwein, J. Groll, F. Tacke, Peptide-functionalized gold nanorods increase liver injury in hepatitis, ACS Nano. 6 (2012) 8767–8777. doi:10.1021/nn302502u.

[79] Y. Hayashi, H. Hatakeyama, K. Kajimoto, M. Hyodo, H. Akita, H. Harashima, Multifunctional Envelope-Type Nano Device: Evolution from Nonselective to Active Targeting System, Bioconjug. Chem. 26 (2015) 1266–1276. doi:10.1021/acs.bioconjchem.5b00184.

[80] J. Wang, R. Bai, R. Yang, J. Liu, J. Tang, Y. Liu, J. Li, Z. Chai, C. Chen, Size- and surface chemistry-dependent pharmacokinetics and tumor accumulation of engineered gold nanoparticles after intravenous administration, Metallomics. 7 (2015) 516–524. doi:10.1039/C4MT00340C.

[81] Z. Zhang, J. Wang, X. Nie, T. Wen, X. Wu, Y. Zhao, C. Chen, Near Infrared Laser Induced Targeted Cancer Therapy Using Thermo-Responsive Polymer Encapsulated Gold Nanorods, (2014). doi:10.1021/ja412735p.

[82] T. Niidome, M. Yamagata, Y. Okamoto, Y. Akiyama, H. Takahashi, T. Kawano, Y. Katayama, Y. Niidome, PEG-modified gold nanorods with a stealth character for in vivo applications, J. Control. Release. 114 (2006) 343–347. doi:10.1016/j.jconrel.2006.06.017.

[83] T. Niidome, Y. Akiyama, K. Shimoda, T. Kawano, T. Mori, Y. Katayama, Y. Niidome, In vivo monitoring of intravenously injected gold nanorods using near-infrared light, Small. 4 (2008) 1001–1007. doi:10.1002/smll.200700438.

[84] F.L. Tansi, R. Rüger, A.M. Kollmeier, C. Böhm, R.E. Kontermann, U.K. Teichgraeber, A. Fahr, I. Hilger, A fast and effective determination of the biodistribution and subcellular localization of fluorescent immunoliposomes in freshly excised animal organs, BMC Biotechnol. (2017) 1–11. doi:10.1186/s12896-017-0327-8.

[85] R. Fernández-Ruiz, M.J. Redrejo, E.J. Friedrich, M. Ramos, T. Fernández, Evaluation of bioaccumulation kinetics of gold nanorods in vital mammalian organs by means of total reflection X-ray fluorescence spectrometry, Anal. Chem. 86 (2014) 7383–7390. doi:10.1021/ac5006475.

[86] J. Ozer, M. Ratner, M. Shaw, W. Bailey, S. Schomaker, The current state of serum biomarkers of hepatotoxicity, Toxicology. 245 (2008) 194–205.

doi:10.1016/j.tox.2007.11.021.

[87] T.M. Allen, P.R. Cullis, Drug delivery systems: entering the mainstream., Science. 303 (2004) 1818–22. doi:10.1126/science.1095833.

[88] S. Yamamoto, A. Kato, Y. Sakurai, T. Hada, H. Harashima, Modality of tumor endothelial VEGFR2 silencing-mediated improvement in intratumoral distribution of lipid nanoparticles, Elsevier B.V, 2017. doi:10.1016/j.jconrel.2017.02.010.

[89] J.W. Sigler, Parenteral gold in the treatment of rheumatoid arthritis., Am. J. Med. 75 (1983) 59–62. http://www.ncbi.nlm.nih.gov/pubmed/6229181 (accessed June 19, 2017).

[90] A. V. Liopo, A. Conjusteau, A.A. Oraevsky, PEG-coated gold nanorod monoclonal antibody conjugates in preclinical research with optoacoustic tomography, photothermal therapy, and sensing, 8223 (2012) 822344. doi:10.1117/12.910838.

[91] P.P. Joshi, S.J. Yoon, W.G. Hardin, S. Emelianov, K. V. Sokolov, Conjugation of antibodies to gold nanorods through fc portion: Synthesis and molecular specific imaging, Bioconjug. Chem. 24 (2013) 878–888. doi:10.1021/bc3004815.

[92] T. Okuno, S. Kato, Y. Hatakeyama, J. Okajima, S. Maruyama, M. Sakamoto, S. Mori, T. Kodama, Photothermal therapy of tumors in lymph nodes using gold nanorods and near-infrared laser light, 172 (2013). doi:10.1016/j.jconrel.2013.10.014.

[93] H. Hatakeyama, S.Y. Wu, Y.A. Lyons, S. Pradeep, W. Wang, Q. Huang, K.A. Court, T. Liu, S. Nie, C. Rodriguez-Aguayo, F. Shen, Y. Huang, T. Hisamatsu, T. Mitamura, N. Jennings, J. Shim, P.L. Dorniak, L.S. Mangala, M. Petrillo, V.A. Petyuk, A.A. Schepmoes, A.K. Shukla, M. Torres-Lugo, J.-S. Lee, K.D. Rodland, A. Fagotti, G. Lopez-Berestein, C. Li, A.K. Sood, Role of CTGF in Sensitivity to Hyperthermia in Ovarian and Uterine Cancers., Cell Rep. 17 (2016) 1621–1631. doi:10.1016/j.celrep.2016.10.020.

[94] Q. Wu, S. Deng, L. Li, L. Sun, X. Yang, X. Liu, L. Liu, Z. Qian, Y. Wei, C. Gong, Biodegradable polymeric micelle-encapsulated quercetin suppresses tumor growth and metastasis in both transgenic zebrafish and mouse models, Nanoscale. 5 (2013) 12480. doi:10.1039/c3nr04651f.

[95] H. Tanaka, Y. Sato, H. Harashima, H. Akita, Cellular environment-responsive

nanomaterials for use in gene and siRNA delivery: molecular design for biomembrane destabilization and intracellular collapse, Expert Opin. Drug Deliv. 5247 (2016) 1–13. doi:10.1517/17425247.2016.1154531.

[96] E.C. Dreaden, I.O. Raji, L.A. Austin, S. Fathi, S.C. Mwakwari, W.H. Humphries, B. Kang, A.K. Oyelere, M.A. El-Sayed, P-glycoprotein-dependent trafficking of nanoparticle-drug conjugates, Small. 10 (2014) 1719–1723. doi:10.1002/smll.201303190.

[97] B. Kang, M.A. Mackey, M.A. El-Sayed, Nuclear targeting of gold nanoparticles in cancer cells induces DNA damage, causing cytokinesis arrest and apoptosis, J Am Chem Soc. 132 (2010) 1517–1519. doi:10.1021/ja9102698.

[98] H.S. Jung, J. Han, J.H. Lee, J.H. Lee, J.M. Choi, H.S. Kweon, J.H. Han, J.H. Kim, K.M. Byun, J.H. Jung, C. Kang, J.S. Kim, Enhanced NIR radiation-triggered hyperthermia by mitochondrial targeting, J. Am. Chem. Soc. 137 (2015) 3017–3023. doi:10.1021/ja5122809.

[99] A. Agarwal, M.A. MacKey, M.A. El-Sayed, R. V. Bellamkonda, Remote triggered release of doxorubicin in tumors by synergistic application of thermosensitive liposomes and gold nanorods, ACS Nano. 5 (2011) 4919–4926. doi:10.1021/nn201010q.

[100] F. Wang, Y.C. Wang, S. Dou, M.H. Xiong, T.M. Sun, J. Wang, Doxorubicin-tethered responsive gold nanoparticles facilitate intracellular drug delivery for overcoming multidrug resistance in cancer cells, ACS Nano. 5 (2011) 3679–3692. doi:10.1021/nn200007z.

[101] D. Wang, Z. Xu, H. Yu, X. Chen, B. Feng, Z. Cui, B. Lin, Q. Yin, Z. Zhang, C. Chen, J. Wang, W. Zhang, Y. Li, Treatment of metastatic breast cancer by combination of chemotherapy and photothermal ablation using doxorubicin-loaded DNA wrapped gold nanorods, Biomaterials. 35 (2014) 8374–8384. doi:10.1016/j.biomaterials.2014.05.094.

[102] M.J. Ware, M. Krzykawska-Serda, J. Chak-Shing Ho, J. Newton, S. Suki, J. Law, L. Nguyen, V. Keshishian, M. Serda, K. Taylor, S.A. Curley, S.J. Corr, J.C. Ho, J. Newton, S. Suki, J. Law, L. Nguyen, V. Keshishian, M. Serda, K. Taylor, S.A. Curley, S.J. Corr, Optimizing non-invasive radiofrequency hyperthermia treatment for improving drug delivery in 4T1 mouse breast cancer model, Sci. Rep. 7 (2017) 43961. doi:10.1038/srep43961.

[103] S. Yamashita, H. Fukushima, Y. Niidome, T. Mori, Y. Katayama, T. Niidome,

Controlled-release system mediated by a retro Diels-Alder reaction induced by the photothermal effect of gold nanorods, Langmuir. 27 (2011) 14621–14626. doi:10.1021/la2036746.

[104] I.C. Pekcevik, L.C.H. Poon, M.C.P. Wang, B.D. Gates, Tunable loading of single-stranded DNA on gold nanorods through the displacement of polyvinylpyrrolidone, Anal. Chem. 85 (2013) 9960–9967. doi:10.1021/ac4027737.

[105] W. Tao, H.S. Gill, M2e-immobilized gold nanoparticles as influenza A vaccine: Role of soluble M2e and longevity of protection, Vaccine. 33 (2015) 2307–2315. doi:10.1016/j.vaccine.2015.03.063.

[106] J. Shen, H.C. Kim, C. Mu, E. Gentile, J. Mai, J. Wolfram, L.N. Ji, M. Ferrari, Z. wan Mao, H. Shen, Multifunctional gold nanorods for siRNA gene silencing and photothermal therapy, Adv. Healthc. Mater. 3 (2014) 1629–1637. doi:10.1002/adhm.201400103.

[107] F. Wang, Y. Shen, W. Zhang, M. Li, Y. Wang, D. Zhou, S. Guo, Efficient, dual-stimuli responsive cytosolic gene delivery using a RGD modified disulfide-linked polyethylenimine functionalized gold nanorod, J. Control. Release. 196 (2014) 37–51. doi:10.1016/j.jconrel.2014.09.026.

[108] E.T. Castellana, R.C. Gamez, D.H. Russell, Label-free biosensing with lipid-functionalized gold nanorods, J. Am. Chem. Soc. 133 (2011) 4182–4185. doi:10.1021/ja109936h.

[109] C. Wang, Y. Chen, T. Wang, Z. Ma, Z. Su, Monodispersed gold nanorod-embedded silica particles as novel Raman labels for biosensing, Adv. Funct. Mater. 18 (2008) 355–361. doi:10.1002/adfm.200700503.

[110] K.C.L. Black, Y. Wang, H.P. Luehmann, X. Cai, W. Xing, B. Pang, Y. Zhao, C.S. Cutler, L. V Wang, Y. Liu, Y. Xia, Radioactive 198Au-Doped Nanostructures with Different Shapes for In Vivo Analyses of Their Biodistribution, Tumor Uptake, and Intratumoral Distribution, (2014) 4385–4394.

[111] N.B. Shah, G.M. Vercellotti, J.G. White, A. Fegan, C.R. Wagner, J.C. Bischof, Blood-nanoparticle interactions and in Vivo biodistribution: Impact of surface peg and ligand properties, Mol. Pharm. 9 (2012) 2146–2155. doi:10.1021/mp200626j.

[112] S. Wilhelm, A.J. Tavares, Q. Dai, S. Ohta, J. Audet, H.F. Dvorak, W.C.W.

Chan, D. Peer, W. Rao, Y. Min, J.M. Caster, M.J. Eblan, A.Z. Wang, A.E. Nel, A. Albanese, P.S. Tang, W.C.W. Chan, T. Endres, X. Huang, I.H. El-Sayed, W. Qian, M.A. El-Sayed, O.S. Wolfbeis, M.F. Attia, M.F. Kircher, X. Guo, C. Shi, J. Wang, S. Di, S. Zhou, W. Gao, J.M. Chan, O.C. Farokhzad, R. Cheng, F. Meng, C. Deng, H.-A. Klok, Z. Zhong, Q. Hu, P.S. Katti, Z. Gu, R. de la Rica, D. Aili, M.M. Stevens, F. Chen, E.B. Ehlerding, W. Cai, Q. Chen, L.Y.T. Chou, K. Zagorovsky, W.C.W. Chan, Y.H. Bae, K. Park, A.Z. Wang, R. Langer, O.C. Farokhzad, K. Park, J. Lazarovits, Y.Y. Chen, E.A. Sykes, W.C.W. Chan, J.W. Nichols, Y.H. Bae, R.K. Jain, T. Stylianopoulos, A.T. Florence, H.S. Choi, J. Liu, J. Liu, M. Yu, J. Zheng, C.M. Dawidczyk, W.L. Chiou, E.A. Sykes, J. Chen, G. Zheng, W.C.W. Chan, C.-C. Tsai, J.F. Kukowska-Latallo, S. Sadekar, A. Ray, M. t-Amsbury, C.M. Peterson, H. Ghandehari, S. Reagan-Shaw, M. Nihal, N. Ahmad, H. Maeda, H. Nakamura, J. Fang, E. Ruoslahti, S.N. Bhatia, M.J. Sailor, H.F. Dvorak, J.A. Nagy, J.T. Dvorak, A.M. Dvorak, J.A. Nagy, H.F. Dvorak, H. Zeng, S. Paku, N. Paweletz, J.A. Nagy, L. Benjamin, H. Zeng, A.M. Dvorak, H.F. Dvorak, S.H. Chang, J.A. Nagy, S.H. Chang, S.C. Shih, A.M. Dvorak, H.F. Dvorak, A. Pettersson, I.J. Fidler, S. Yano, R.D. Zhang, T. Fujimaki, C.D. Bucana, C. Sundberg, J.A. Nagy, S.C. Shih, W.H. Wong, A.M. Dvorak, H.F. Dvorak, J.A. Nagy, A.M. Dvorak, H.F. Dvorak, H. Kobayashi, R. Watanabe, P.L. Choyke, U. Prabhakar, Y. Matsumura, H.A. Maeda, H.F. Dvorak, S. Hobbs, A.M. Dvorak, D. Feng, J.A. Nagy, J. Hipp, H.F. Dvorak, A.M. Dvorak, M.W. Pickup, J.K. Mouw, V.M. Weaver, C. Box, S.J. Rogers, M. Mendiola, S.A. Eccles, S.A. Eccles, P. Alexander, C.-H. Heldin, K. Rubin, K. Pietras, A. Ostman, M.A. Swartz, A.W. Lund, S.D. Perrault, C. Walkey, T. Jennings, H.C. Fischer, W.C.W. Chan, V.P. Chauhan, F. Yuan, A. Albanese, A.K. Lam, E.A. Sykes, J. V. Rocheleau, W.C.W. Chan, X. Huang, S. Kunjachan, C.H.J. Choi, C.A. Alabi, P. Webster, M.E. Davis, S. Gordon, P.R. Taylor, H.C. Fischer, T.S. Hauck, A. bal, W.C.W. Chan, S. Huang, L.C. Davies, S.J. Jenkins, J.E. Allen, P.R. Taylor, A. Syed, W.C.W. Chan, P.C. Patel, H. Wang, L. Wu, B.M. Reinhard, T. Cedervall, C.D. Walkey, W.C.W. Chan, A. Albanese, C.D. Walkey, J.B. Olsen, H. Guo, A. Emili, W.C.W. Chan, C.D. Walkey, W.H. de Jong, W.M. Deen, M.J. Lazzara, B.D. Myers, M.A. Venkatachalam, H.G. Rennke, A. V. Nair, E.J. Keliher, A.B. Core, D. Brown, R. Weissleder, G. Pillai, V.J. Venditto, F.C. Szoka, T.M. Allen, P.R. Cullis, Y.

Barenholz, R.C.F. Leonard, S. Williams, A. Tulpule, A.M. Levine, S. Oliveros, V.P. Chauhan, W. Jiang, Y. Huang, Y. An, B.Y.S. Kim, T.D. Tailor, C. V. Pastuskovas, M. Dobosz, V. Ntziachristos, W. Scheuer, S. Strobel, M. Roger, L. Li, H. Cheng, Q. Hu, J.A. MacDiarmid, S.J. Park, N. Doshi, D. Akin, S.J. Kuhn, S.K. Finch, D.E. Hallahan, T.D. Giorgio, M. Cui, A.J. Gormley, P. Diagaradjane, Y. Ohara, N. van Rooijen, A. Sanders, P. Diagaradjane, A. Deorukhkar, J.G. Gelovani, D.M. Maru, S. Krishnan, A. Parodi, J.-G. Piao, P.L. Rodriguez, S. Barua, S. Mitragotri, J. Pascal, E.J. Koay, K. Shao, J.E. Zuckerman, A.D. Bangham, M.M. Standish, J.C. Watkins, Analysis of nanoparticle delivery to tumours, Nat. Rev. Mater. 1 (2016) 16014. doi:10.1038/natrevmats.2016.14.

Curriculum Vitae

Name:	West Kristian D. Paraiso
Nationality:	Filipino (Philippines)
Birth date:	Aug. 7, 1987
Birth place:	Makati, Metro Manila, Philippines

Educational background

June 2004 – April 2009	Bachelor of Science in Industrial Pharmacy
	College of Pharmacy, University of the Philippines-Manila
Jan. 2010	Pharmacist Licensure Examination
Jan. 2010 – April 2012	Master of Science in Chemistry
	College of Science, De La Salle University
April 2014 – Sept. 2014	Research Student
	Laboratory for Molecular Design of Pharmaceutics
	Faculty of Pharmaceutical Sciences, Hokkaido University
Oct. 2014 – *present*	Doctor of Life Science, *candidate*
	Biomedical and Pharmaceutical Science Course
	Graduate School of Life Science, Hokkaido University

Professional background

June 2009 – Oct. 2011	Instructor
	College of Pharmacy, University of the Philippines-Manila
Jan. 2012 – Dec. 2012	Senior Research Assistant
	Marine Science Institute, University of the Philippines-Diliman
Jan. 2013 – March 2014	Assistant Professor
	College of Pharmacy, University of the Philippines-Manila